Paulina Piller, BSc

Mode of action of LL-37 derived antimicrobial peptides in Enterococcus hirae

MASTER'S THESIS

to achieve the university degree of

Master of Science

Master's degree programme: Biochemistry and Molecular Biomedical Sciences

submitted to

Graz University of Technology

Supervisor

Assoz. Prof. Dipl.-Ing. Dr.techn. Karl Lohner

Institute of Molecular Biosciences
University of Graz

Graz, July 2019

AFFIDAVIT

I declare that I have authored this thesis independently, that I have not used other than the declared sources/resources, and that I have explicitly indicated all material which has been quoted either literally or by content from the sources used. The text document uploaded to TUGRAZonline is identical to the present master's thesis.

26.07.2019
Date

P. Bille
Signature

ACKNOWLEDGEMENTS

At this point, I want to thank everyone, who helped me during my master thesis.

First and foremost, I would like to express my sincere gratitude to Prof. Dipl.-Ing. Dr.techn. Karl Lohner for giving me the opportunity to do my master thesis in his research group and for his helpful suggestions, his constructive criticism as well as the great cooperation and the review of this thesis. I would also like to thank Mag. Dr.rer.nat. Nermina Malanovic, who supervised me throughout my time as her master student. She gave me a lot of support and great suggestions and introduced me to the topic of membrane mimetics and antimicrobial peptides and all the working procedures in the laboratory.

Besides my supervisors, I want to thank all colleagues of this institute for their help.

Finally, I am grateful to my mother, my sister and my boyfriend for their moral support during my whole studies.

TABLE OF CONTENTS

ABSTRACT

Multidrug antibiotic resistance of bacterial strains is an increasingly serious problem for the treatment of infectious diseases. The development of antimicrobial agents against multidrug resistant (MDR) bacteria is an important challenge in modern society. Here, we studied the mode of action of three cationic antimicrobial peptides (AMPs) derived from human cathelicidin LL-37: OP-145, SAAP-148 and I12K using the Gram-positive bacterial strain *Enterococcus hirae* as well as model membranes mimicking the bacterial plasma membrane. The major lipid species of *E. hirae* are negatively charged phosphatidylglycerol (PG) and cardiolipin (CL).

We determined the lethal peptide concentration using *E. hirae*, which is 0.1 µM for SAAP-148, 3.2 µM for OP-145 and 51.2 µM for I12K. Electrostatic interactions between the cationic antimicrobial peptides and the anionic surface of *E. hirae* as well as the model membranes were examined by Zeta-potential measurements showing that the peptides did not alter the surface charge of *E. hirae* significantly. Nevertheless, the negative surface charge of PG and PG/CL decreased in a dose-dependent manner and reached zero at peptide concentrations at which full membrane permeabilization was already induced. This indicates that the peptides easily penetrate the cell wall and not all membrane charges need to be covered by the peptides before total membrane collapse. Microscopy showed accumulation of the peptides in septal or polar regions of the membrane reflecting changes in membrane fluidity in agreement with observations from DSC measurements. Loss of cytoplasmic material at defined areas of the membrane led to shrinkage of the cells.

These data demonstrate that OP-145 and SAAP-148 are effective antimicrobial peptides, whereby SAAP-148 is a stronger AMP as it neutralizes the membrane surface faster and kills bacteria at a significantly lower concentration than OP-145. I12K exhibits very weak bactericidal activity against *E. hirae*. We propose that the disruption of the bacterial membrane by OP-145, SAAP-148 and I12K will most likely occur by pore formation. However, further investigations are recommended to fully understand their mode of action.

ZUSAMMENFASSUNG

Multiresistenzen von Bakterien gegen Antibiotika stellen ein ernsthaftes, stetig wachsendes Problem für die Behandlung von Infektionen dar. Die Entwicklung antimikrobieller Substanzen ist eine bedeutsame Herausforderung der heutigen Zeit. In dieser Arbeit haben wir den Wirkungsmechanismus von drei positiv geladenen antimikrobiellen Peptiden (AMP) OP-145, SAAP-148 und I12K abgeleitet vom humanen Cathelicidin LL-37 erforscht. Als Modelle dienten das Gram-positive Bakterium *Enterococcus hirae* und bakterielle Modellmembranen. Negativ geladenes Phosphatidylglycerol (PG) und Cardiolipin (CL) sind die Hauptlipidspezies von *E. hirae*.

Die letale Peptidkonzentration für *E. hirae* ist 0.1 µM für SAAP-148, 3.2 µM für OP-145 und 51.2 µM für I12K. Elektrostatische Wechselwirkungen zwischen den kationischen AMPs und der anionischen Oberfläche von *E. hirae* sowie den Modellmembranen wurden mittels Zeta-Potenzials Messungen untersucht. Diese zeigten keine signifikanten Veränderungen der Oberflächenladung von *E. hirae*. Im Gegensatz hierzu nahm die negative Oberflächenladung von PG und PG/CL dosisabhängig ab und erreichte schließlich ein Zeta-Potenzial von Null. Bei diesen Peptidkonzentration wurde bereits eine vollständige Permeabilisierung der Membran induziert, was auf eine ungehinderte Penetration der Peptide durch die Zellwand hindeutet. Nicht alle Ladungen der Membran müssen durch die Peptide abgedeckt werden, bevor ein totaler Zusammenbruch der Membran erfolgt. Mikroskopie Experimente zeigten, dass die Peptide in Bereichen von Septum und Polen innerhalb der Membran akkumulieren. Das deutet auf eine veränderte Membranfluidität hin in Übereinstimmung mit DSC Messungen. Der Verlust zytoplasmatischen Materials führte zu einem Schwund der Zellen.

Unsere Daten zeigen, dass OP-145 und SAAP-148 sehr effektiv wirken, wobei SAAP-148 durch seine schnellere Neutralisierung der Membranoberfläche und die signifikant geringere letale Konzentration als stärkeres AMP anzusehen ist. I12K weist hingegen eine sehr schwache bakterizide Wirkung. Wir postulieren eine Porenbildung, die höchstwahrscheinlich bei der Zerstörung der bakteriellen Membran durch OP-145, SAAP-148 und I12K auftritt. Um den Mechanismus der Peptide vollständig zu verstehen, werden jedoch noch weitere Untersuchungen notwendig sein.

1. INTRODUCTION

Nowadays, the worldwide re-emergence of infections, the increase of pathogenic bacteria and the subsequent rising incidence of multidrug resistance of bacterial strains against commercially available antibiotics is an increasingly serious problem for the treatment of infectious diseases like pneumonia, urinary tract infections and bloodstream infections [1–3]. Multidrug-resistant (MDR) strains that belong to the so-called ESKAPE (*Enterococcus faecium*, *Staphylococcus aureus*, *Klebsiella pneumoniae*, *Acinetobacter baumannii*, *Pseudomonas aeruginosa* and *Enterobacter* species) panel cause nosocomial infections leading to death of substantial numbers of patients [4]. A high percentage of hospital-acquired infections is caused by the Gram-positive methicillin resistant *Staphylococcus aureus* (MRSA) strain [1,3]. Hence, antibiotic resistance is one of the biggest threats to global health and leads to higher medical costs, longer hospital stays and increased mortality [5]. It is ranked as a priority disease by the World Health Organization. This creates an urgent demand for new alternatives to antibiotics and a shift to a treatment with second-line antibiotics [1,6].

1.1. ANTIBIOTICS – MODE OF ACTION AND RESISTANCE MECHANISMS

Generally, conventional antibiotics act by binding to specific receptors and inhibiting cellular processes by the interference with cell processes such as protein or cell wall biosynthesis and DNA replication [7]. Some examples for commercial antibiotics are Penicillin (inhibits cell wall biosynthesis) [1,7], Clindamycin (protein biosynthesis 50S inhibitor) [1], Amikacin (protein biosynthesis 30S inhibitor) [1], Quinolones (inhibits DNA gyrase) [1,7], Rifampin (inhibits RNA polymerase) [1] and Sulfonamides (inhibits folic acid metabolism) [1,7]. Many different strategies of antibiotic resistance have been reported, such as decreased uptake or increased efflux of the antibiotic from the cell, modification of target molecules or antibiotic inactivation by specific enzymes (β-lactamases, aminoglycoside-modifying enzymes and chloramphenicol acetyltransferases) [7]. New drugs that act in the same way as antibiotics based on receptor binding will more likely induce resistance. Therefore, alternative drugs with novel mode of actions are desired [1,7].

1.2. ALTERNATIVE TO ANTIBIOTICS – ANTIMICROBIAL PEPTIDES

One alternative to antibiotics are antimicrobial peptides (AMPs). AMPs represent an emerging strategy based on their different modes of action compared to conventional antibiotics. These peptides can provide a first line of defense against pathogenic microorganisms as they are effector molecules of the innate immunity [1]. Within the last decade, research on antimicrobial peptides has markedly expanded as reflected with more than 3000 peptides of natural or synthetic origin reported to date by the Antimicrobial Peptide Database [8]. AMPs are found in animals, plants, bacteria, fungi, protists and archaea, whereby animals are the biggest source of antimicrobial peptides. They can be categorized in different groups, such as in anti-bacterial peptides, anti-biofilm, anti-cancer or anti-viral AMPs [8,9].

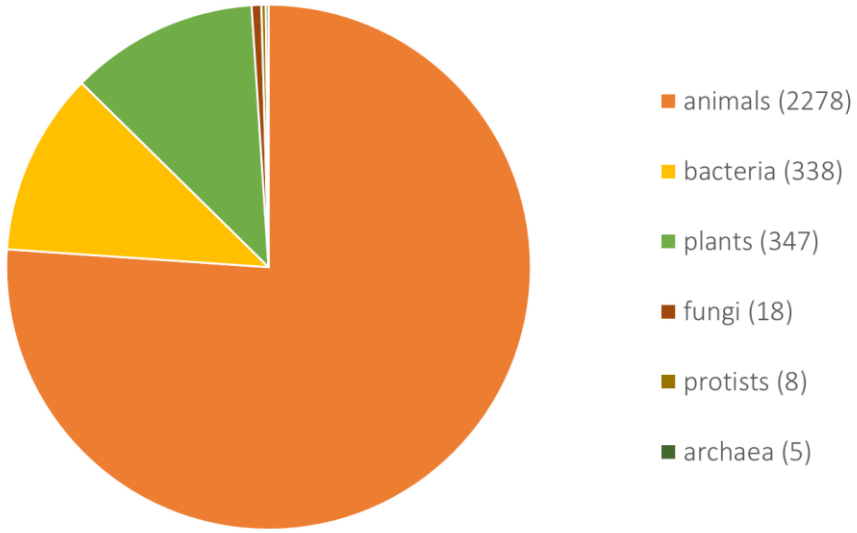

Figure 1. Sources of antimicrobial peptides (total 2994) as of May 2019 from the antimicrobial peptide database. Numbers obtained from http://aps.unmc.edu/AP/, accessed on 16 May 2019.

On a structural basis, the peptides show a wide variety ranging from α-helical, β-sheet, extended to loop among different AMPs [1,10]. Although AMPs are a varying group of molecules in respect of sequence, structure and sources, there are some properties they all have in common [9]. Such peptides are generally, small, amphipathic, resulting from the segregation of apolar and polar residues upon secondary structure formation, and have high levels of cationic residues. Their positive net charge ranges from +2 to +13. According to Malanovic and Lohner [11], the amino acid composition of AMPs determines the physicochemical properties of the peptide concerning charge, hydrophobicity, amphipathicity,

H-bonding capacity and flexibility. Hydrophobicity is the key to insertion into and perturbation of the membrane [3,11]. AMPs affect depolarization, destabilization and permeabilization of the bacterial membrane [12]. However, the mode of action of AMPs consists of three main steps – targeting the microbial cytoplasmic membrane, interaction with the lipid matrix and subsequent membrane permeabilization. The peptide and lipid composition of the membrane strongly affects the antimicrobial activity [2,9].

In respect of antimicrobial peptides, bacterial resistance is less likely to occur because of their specific cell killing mechanisms that are not mediated through specific receptor interactions. To become resistant, substantial modifications of the lipid composition would be necessary, which in turn affects bacterial cell viability [1]. Boman states another advantage of AMPs concerning bacterial resistance is their ability to destroy bacteria within minutes. An effective defense is enabled as the killing rate is faster than the bacterial growth rate [13].

1.3. HUMAN ANTIMICROBIAL PEPTIDE – CATHELICIDIN LL-37

Besides *E. hirae*, the three synthetic peptides OP-145, SAAP-148 and I12K, which were already used in other studies, are the focus of this study (Malanovic et al. [2], de Breij et al. [4,12], Ming and Huang [14]). They are all derived from the human AMP cathelicidin LL-37. It is the only human cathelicidin-derived AMP. Indeed, it is one of the best studied major human AMPs that play a constitutive role in the immune system defending against local and systemic infections. This peptide exhibits a wide spectrum of bactericidal activities against Gram-positive as well as Gram-negative bacteria by destroying the bacterial membrane [2,4]. It is expressed in the epithelial cells of the skin, testis, gastrointestinal tract, the respiratory tract and in the leukocytes. According to Dürr et al. [15], LL-37 has additional defensive roles like inflammatory response regulation or promotion of re-epithelialization and wound closure [15]. Based on its amphipathicity LL-37 interacts electrostatically with the anionic bacterial membrane. The peptides' modes of action are depolarization, destabilization and penetration of the cell membrane, formation of transmembrane pores and subsequently lysis of bacterial cells. Mammalian cells are protected against these pore-forming effects of LL-37 by their membrane compound cholesterol [16]. The sequence of LL-37 is LLGDFFRKSKEKIGKEFKRIVQRIKDFLRNLVPRTES [15]. Figure 2 presents the NMR structure (A) [17] and the helical wheel projection (B) [18] of the peptide that shows the region 12-29 of the

helix. All in all, the peptide has a net charge of +6 at physiological pH, 37 amino acids and is composed of two helical domains with its break point centered at amino acid K12 [18]. LL-37 consists of a hydrophilic region as well as a hydrophobic part, that interacts with the bacterial membrane [15]. The introduction of some modifications in the sequence of LL-37 has led to the design of three synthetic antimicrobial peptides with improved bactericidal properties – OP-145, SAAP-148 and I12K.

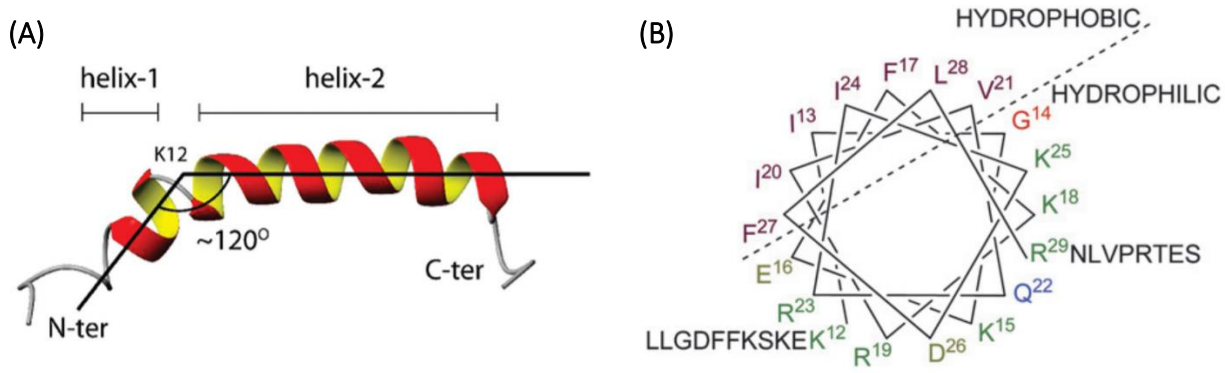

Figure 2. Structure of the human antimicrobial peptide LL-37. (A) NMR structure of LL-37 showing the angle between the two helical domains and the break point centered at K12 [17] (B) Helical wheel projection of the region 12-29 as an amphipathic helix. N- (residues 1-11) and C- (residues 30-37) termini residues are unstructured [18].

1.4. SYNTHETIC ANTIMICROBIAL PEPTDES – OP-145, SAAP-148, I12K

The peptides' sequences (OP-145, SAAP-148, I12K) are derived from LL-37. Sequence modifications, amino acid replacements at the C-terminus and protection against proteolytic degradation should improve antimicrobial activity. For OP-145 the sequence is acetyl-IGKEFKRIVERIKRFLRELVRPLR-amide, for SAAP-148 acetyl-LKRVWKRVFKLLKRYWRQLKKPVR-amide and for I12K it is acetyl-IGKEFKRIVERKKRFLRELVRPLR-amide. Each peptide is composed of 24 amino acids and has a hydrophobic and a hydrophilic region. In contrast to OP-145 (+6) and I12K (+7), SAAP-148 has a higher net charge of +11 at physiological pH. The hydrophobic region of SAAP-148 is bigger. Consequently, it can insert deeper into membrane than OP-145 and I12K, resulting in a stronger membrane disruption and killing at a significantly lower concentration [19]. The peptide I12K has in principal the same sequence as OP-145 with one exception, I12K has a lysin (K) instead of an isoleucine (I) at position 12 that leads to a break in the hydrophobic region (Figure 3) [20].

(A) OP-145

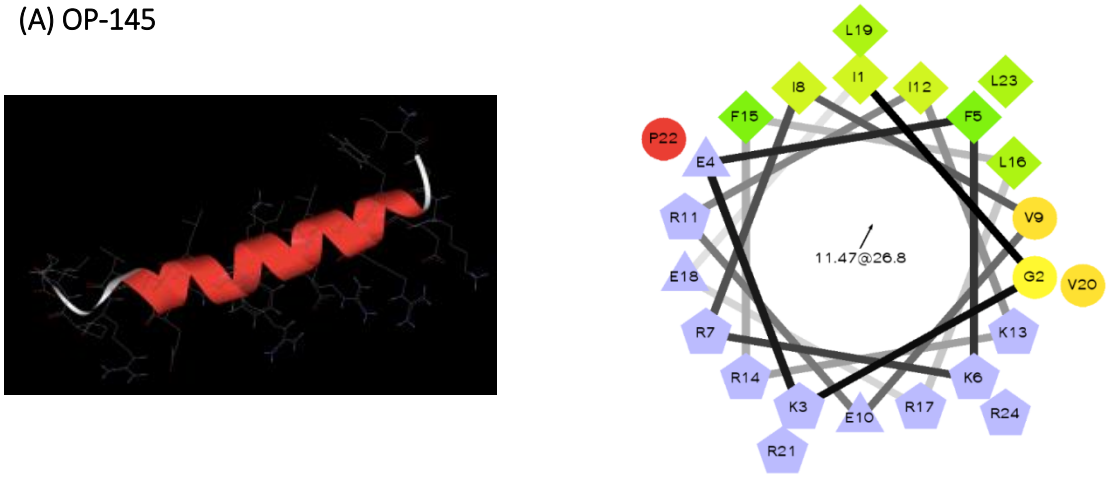

(B) SAAP-148

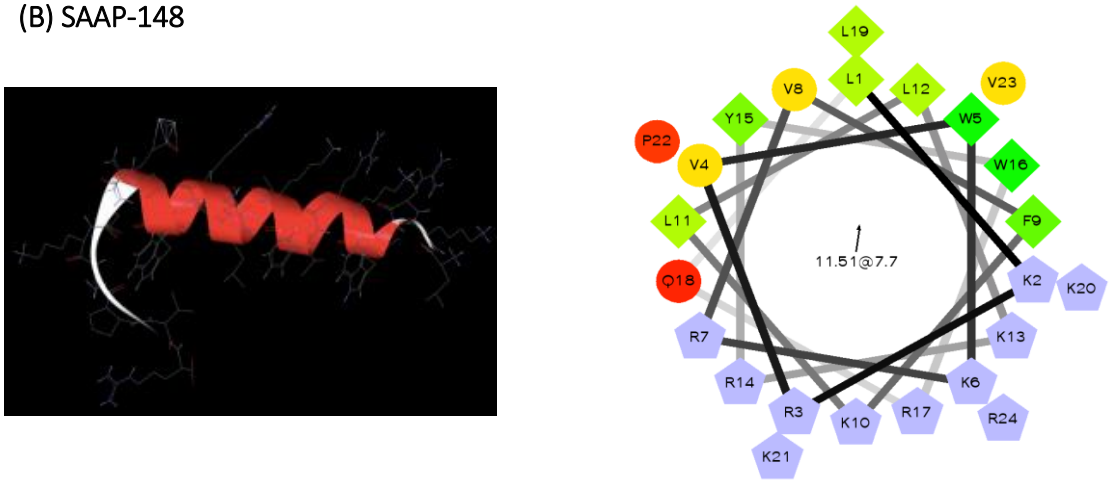

(C) I12K

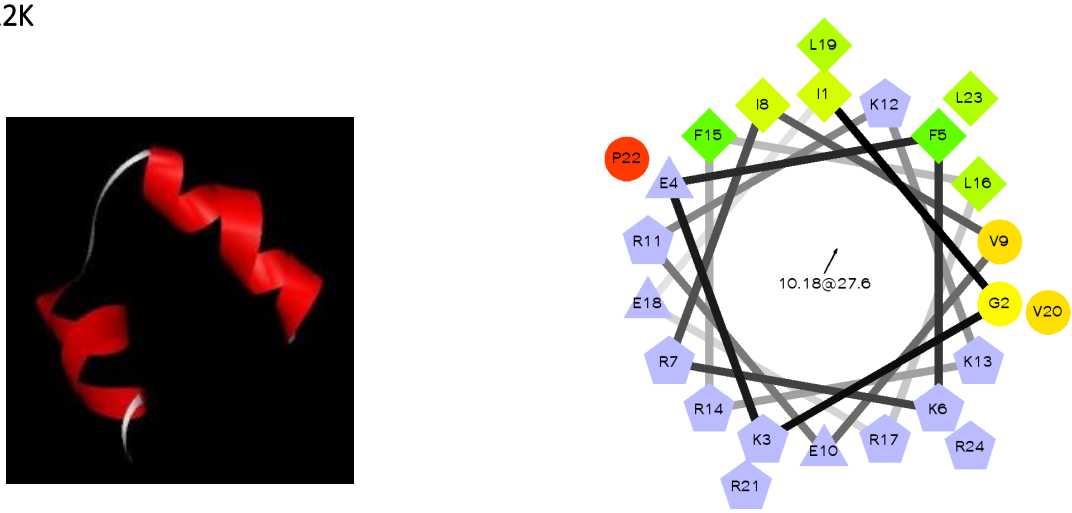

Figure 3. α-helical structure by Mobyle@RPBS (left panel) and helical wheel projection (right panel) of the antimicrobial peptides (A) OP-145, (B) SAAP-148 and (C) I12K

Earlier studies have already investigated the mode of action of OP-145, SAAP-148 and I12K against *Escherichia coli* and *Staphylococcus aureus*. *E. coli* can cause urinary tract infections,

prostate infections and diarrheal diseases [5]. *S. aureus* causes hospital-acquired infections such as skin infections followed by sepsis, in the worst case even death [3]. SAAP-148 permeabilizes the cytoplasmic membrane of these bacteria, leading to death [4]. In accordance with Haisma et al. [21], OP-145 shows high efficiency against MRSA, eliminating biofilm-associated bacteria, without affecting human epidermal models. Further studies with *S. aureus* biomaterial-associated infections (BAI) from de Breij et al. [12] confirm that concerning *Staphylococcus aureus* OP-145 does display bactericidal activity. OP-145 has proven to efficiently treat chronic ortitis in patients [12] and exhibits high antimicrobial activity against *S. aureus* [2,12]. Regarding *E. coli* OP-145 kill bacteria by permeabilizing the membrane [2]. Data from I12K have not been published yet.

1.5. BACTERIAL CELL MEMBRANES

Biomembranes are a fundamental permeability barrier of all cells. They act as targets of AMPs. Initial binding of the peptides to the bacterial membrane is caused by the attraction to the bacterial surface by electrostatic interactions between the positively charged peptides and the anionic cell wall components like lipopolysaccharides (LPS) in Gram-negative and lipoteichoic acids (LTA) in Gram-positive bacteria [3]. The affinity to phosphatidylglycerol (PG) is supposed to determine the interactions between antimicrobial peptides and the target membranes since the plasma membrane of Gram-positive bacteria consists of a high amount of negatively charged PG [2]. In contrast, Gram-negative bacteria are composed of a lower quantity of PG [11]. Discrimination between bacterial and host (human or mammalian or eukaryotic) cell membrane is due to their different surface charges, the latter being not charged. Animal membranes are composed of zwitterionic phospholipids such a phosphatidylcholine PC, sphingomyelin or cholesterol [9,22].

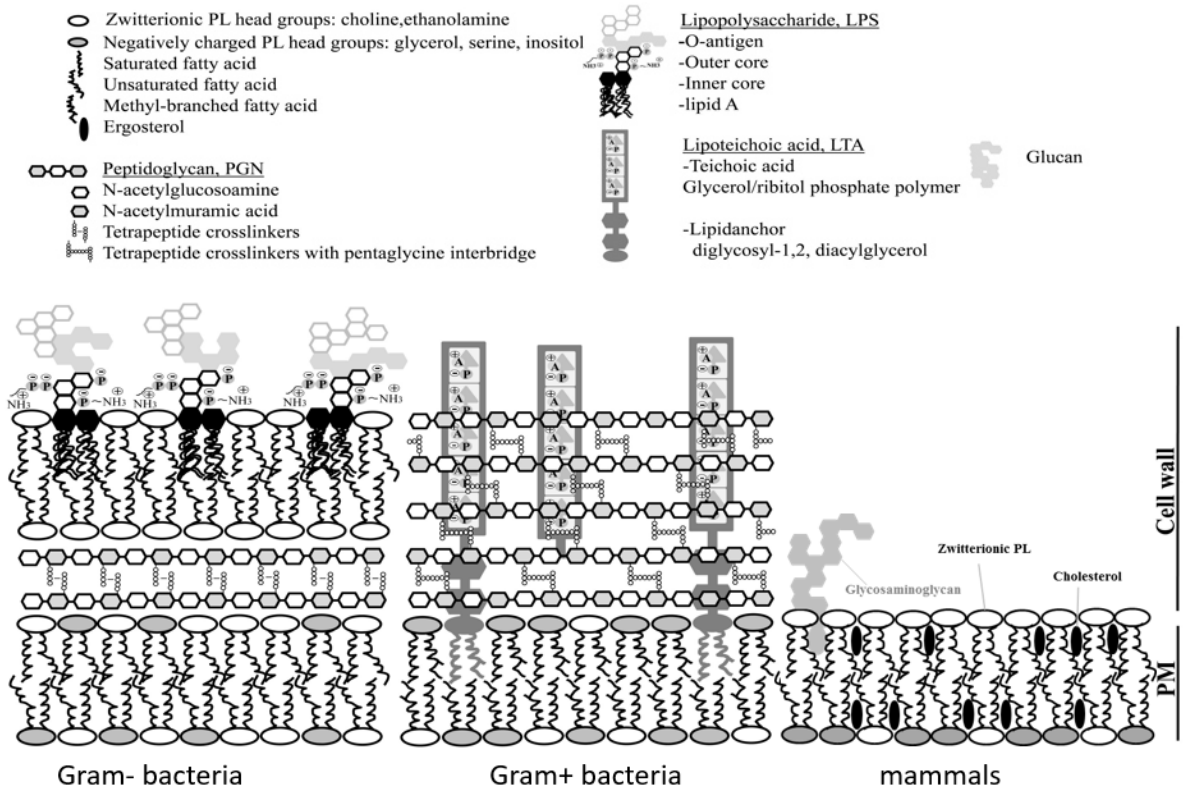

Figure 4. Cell envelope of Gram-negative bacteria, Gram-positive bacteria and mammals. Modified figure from [11].

Bacterial plasma membranes are negatively charged due to anionic phospholipids. Gram-positive bacterial plasma membrane (e.g. *S. aureus*) is made of 95% PG and 5% cardiolipin (CL), whereas Gram-negative bacterial membrane (e.g. *E. coli*) consists of 75% phosphatidylethanol (PE) and 25 % PG [3]. Gram-positive and Gram-negative bacteria distinguish in many features. However, one characteristic both classes share is that the cytoplasmic membranes are encompassed by a cell wall. Gram-positive bacteria like *Enterococcus hirae* (*E. hirae*) possess a simple lipid bilayer membrane surrounded by a thick peptidoglycan (PGN) layer and lipoteichoic acid (LTA). In contrast, Gram-negative bacteria's cell envelope is a complex structure composed of three different layers – an inner and outer membrane as well as an intervening very thin peptidoglycan layer in the periplasmic space. The outer membrane of Gram-negative bacteria consists of lipopolysaccharides (LPS) that form a distinctive, highly asymmetric membrane structure. *Escherichia coli* (*E. coli*) is a representative of this class of bacteria. LTA and LPS mainly contribute to the negative charge in the cell surface of bacteria. (Figure 4) [11,23]. The cell wall composition of Gram-positive bacteria is described more detailed in Chapter 1.6.

1.6. GRAM-POSITVE BACTERIA – *ENTEROCOCCUS HIRAE*

In this study, we want to assess the mode of action of antibacterial peptides against the Gram-positive bacterial strain *Enterococcus hirae*. This strain was selected because it is ranged in safety class one and is therefore considered as non pathogenic. In further consequence, this research serves as a template for additional investigations with pathogenic Gram-positive strains or other *Enterococci* strains like *Enterococcus faecium* and *E. faecalis*, which have attained great clinical significance. According to Dicpinigaitis et al. [24], infections with *E. hirae* have rarely been reported in humans, but they are not that uncommon in mammals and birds. There are some cases described with *Enterococcus hirae* bacteremia associated with acute cholecystitis, acute pancreatitis and septic shock as well as endocarditis [24,25].

Enterococci belong to the group of Gram-positive bacteria. They are part of the microbiota of humans and animals. *E. faecium* (10%) and *E. faecalis* (80%) species are the major enterococcal isolates in humans. They can cause human infections like urinary tract infections, endocarditis and bacteremia. As opposed to this, *E. hirae* is rarely isolated from humans (1%) [25].

The adaption to the anaerobic conditions in the gastrointestinal tract has led to a survival strategy of Enterococci against the defense mechanism of the mammalian host, which is the depletion of environmental iron to hinder bacterial growth. The enterococcal counter-strategy is an iron-independent metabolism [26].

The Gram-positive bacterial cell wall primarily consists of three main constituents: a peptidoglycan backbone, teichoic acid and cell wall polysaccharides collectively termed as anionic polymers and wall-associated as well as wall-anchored proteins. The proteins only comprise about 10% of the total cell wall weight, whereby the PGN backbone and the anionic polymers comprise 90%. Polysaccharides, teichoic acid and surface-anchored proteins are covalently attached to the cell wall PGN, while lipoproteins and lipoteichoic acid are tethered to membrane lipids via covalent linkage [27].

The enterococcal wall is predominantly composed of peptidoglycan (PGN) with its repeating disaccharide units *N*-acetylmuramic acid-(β1-4)-*N*-acetylglucosamine (MurNAc-GlcNAc; NAM-NAG) that are cross-linked by short stem peptides which are appended to MurNAc residues [27,28]. The cell wall chemistry of *E. hirae* displays following aspects: insertion of an uncharged bridge between tail-to-tail peptide bond; D-γ-glutamyl acid residues have an aminated α-

carboxyl group; presence of a L-lysine with a missing carboxyl group resulting in a single negative net charge of the wall cross bridging peptide. A poly-amino aspartic bridge connects the ε-amino group of the lysine with the carboxyl group of the other chain's D-alanine. Furthermore, the enterococcal wall displays an inability to stretch because of intramolecular forces keeping the cell wall in a compact configuration [26].

The PGN backbone is represented as an ordered, right-handed helix consisting of three NAG-NAM pairs per helical turn leading to a three-fold symmetry of the stem peptides oriented around the axis. This, in turn, results in a cross-linkage of one single peptidoglycan to three neighboring strands. The stem peptide is composed of L-Ala-D-Glu-L-Lys-D-Ala-D-Ala, equal to many other Gram-positives [27].

In addition to glycan strand polymerization and cross-linking by transpeptidases, cell wall synthesis is mediated through autolytic enzymes, the muramidases, which were firstly described by Shockman and coworkers in the 1960s [29]. These peptides represent cell wall associated proteins. They target and cleave NAG-NAM residues. In contrast, cell wall anchored (CWA) proteins become fixed to the cell wall after secreting through the cell membrane. CWA proteins contain specific motifs that are detected by membrane-bound transpeptidases, so-called sortases which conduct covalent anchoring of the proteins to the cell wall [27].

The lipid-anchored moieties comprise lipoproteins and lipoteichoic acid. Enterococcal lipoproteins capture small molecules and facilitate their transport inside the cell. Lipoteichoic acid is composed of a glycerol phosphate teichoic acid polymer with kojibiose substitutions (disaccharide of 1, 2-linked glucose), whereby D-alanylations are interspersing along the glycerol backbone. LTA is attached to the membrane by the enzymes BgsA and BgsB. As opposed to this, the linkage of cell wall teichoic acid (WTA) is mediated through N-acetyl muramic acid residues in the PGN. Either ribitolphosphate or glycerolphosphate repeating units that are substituted by D-alanylation or glycosylation are the main constituents of WTA polymers [27].

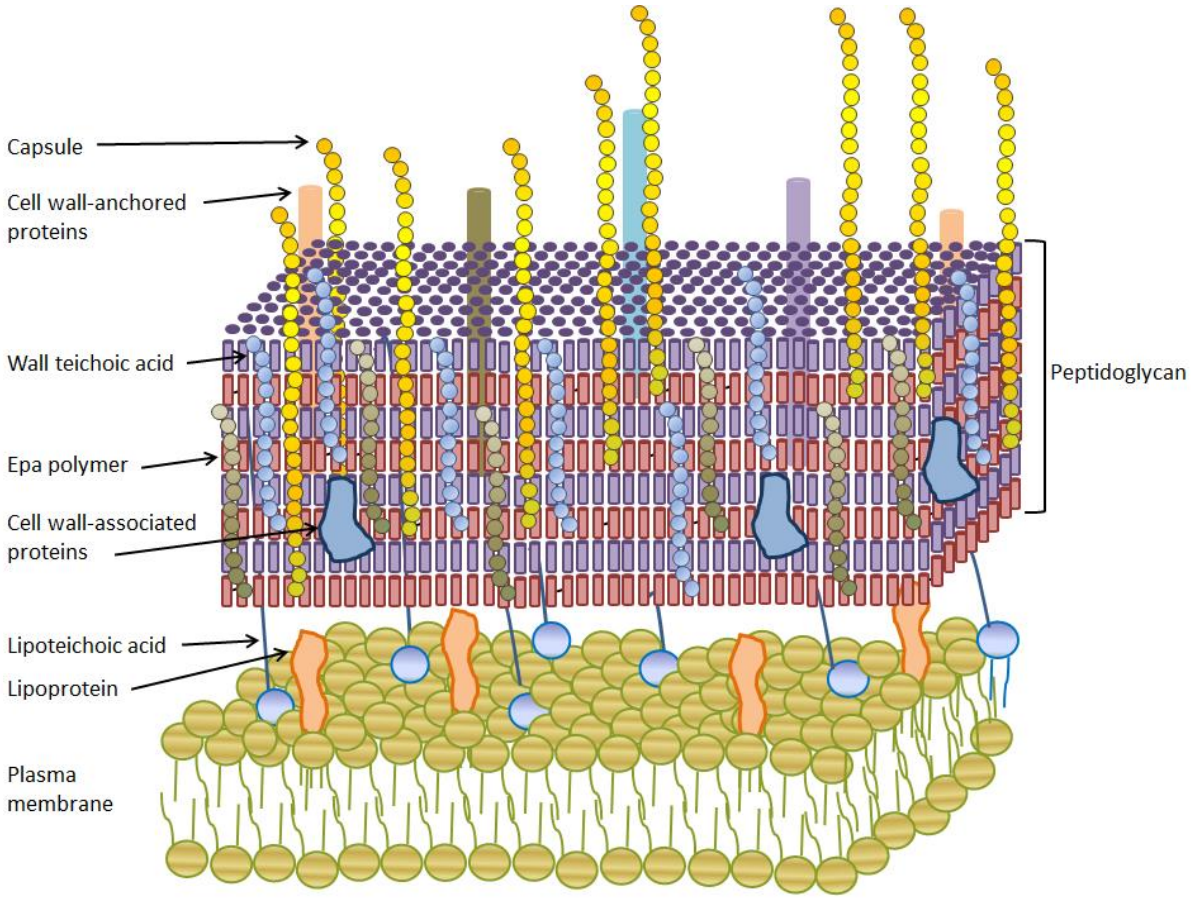

Figure 5. Model of the enterococcal cell wall consisting of the peptidoglycan layer and the plasma membrane [27].

Newly formed *E. hirae* cells exhibit an American football-like shape with a high surface to volume ratio that is more increased the more the pole is stretched. Enterococcal growth is zonal and is marked by an equatorial annulus formation by the addition of new wall material. The annular septum is subsequently split into two new prolate poles in one plane by autolysin action, whereby the septum's material becomes a constituent of the externalized pole [26]. Autolysins are thought to play an important part in cell wall growth and cell division causing autolysis of Enterococci because of bond hydrolyzation of peptidoglycan in the cell wall as it is demonstrated for the enterococcal strain *E. hirae* ATCC 9790 by Shockman [30]. The ultimate pole shape is achieved when the wall is exteriorized and the planar septum split. Reworking of the wall after splitting does not occur. The partial emergence of cell chains results from the described enterococcal growth habit [26].

The formation of new growth zones as part of the cell division can be conducted in a symmetrical or asymmetrical manner. It can be distinguished between slow and more rapid growth rates, whereby new growth sites arise shortly after cell division in the first case and

before division in the second case. As the ongoing protoplasmic growth cannot be supported by increasing the cell's volume fast enough, the initiation of new growth zones is performed. Depending on the number (one or two) of wall bands split one or two new growth zones are formed. According to Koch [26] turgor pressure, which is the force within the cell pushing the bacterial plasma membrane against the cell wall, may act a part in growth zone formation. The solid wall, with its unalterable dimensions, hinders the cell enlargement that would be triggered by the turgor pressure [26]. In contrast to Enterococci, *S. aureus* cells are enlarged rather primarily in the splitting process of the mother cell, but not during the cell cycle. Monteiro et al. claimed that the enlargement of staphylococcal cells requires either peptidoglycan synthesis, which occurs in most cases at the division septum or autolysis or both processes combined [31].

There exist two models describing the connection between pole and septum. The zonal dome model suggests that the incorporation of the septal wall into the external pole wall is the basis for the accurate prediction of the pole shape. The split-and-splay model supposes that the septal wall area is twisted instead of becoming exteriorized or enlarged by splitting. For this model, there exists a requirement for replacement-synthesis to create an additional wall for the pointed, prolate pole [26].

1.7. PEPTIDE-MEMBRANE-INTERACTIONS

For interaction between antimicrobial peptides and bacteria, there are not only peptide characteristics, but also bacterial characteristics that play a central role in binding and selecting towards bacteria. This includes in particular the negative charge resulting from anionic phospholipids and the transmembrane potential which is usually higher in bacteria than in mammal cells [9,23]. The high binding capacity of antimicrobial peptides, such as OP-145, SAAP-148 and I12K, impairs a high potential to neutralize bacterial cell wall components, as reported by Malanovic et al. [2]. According to Bechinger and Lohner [32], peptide-membrane interactions and the subsequent membrane morphologies are influenced by many other factors, like peptide-to-lipid ratio, a detailed membrane composition, temperature, hydration and buffer composition [32]. Furthermore, it should be considered that the different cell wall components have different impacts on the partitioning of antimicrobial peptides. As the PGN is relatively porous and acts like a sponge, the penetration of the cell wall by small molecules

like antimicrobial peptides is facilitated and subsequent interaction with the phospholipid bilayer occurs. As opposed to this, LTA may act either as a ladder leading the AMPs to the cytoplasmic membrane or as an entrapper, since the anionic LTA exhibits a strong attraction potential for positively charged molecules like AMPs [33].

1.8. MODELS FOR THE MODE OF ACTION OF ANTIMICROBIAL PEPTIDES

After the initial electrostatic interaction, the peptides accumulate at the bacterial surface and self-assemble on the membrane after reaching a certain concentration [9]. At this point, several models have been used to describe the peptides' mode of action. The models can be classified into two categories: transmembrane pore models [9,32] and non-pore models [9] (Figure 6). The former models can be further subclassified into the toroidal pore and the barrel-stave pore models [9,22,34]. In the barrel stave model, the peptides are initially oriented parallel to the lipid bilayer, but insert perpendicular into the membrane above a certain threshold concentration. In the toroidal pore model, AMPs also insert perpendicularly in the bilayer but without specific peptide-peptide interactions. The main difference between these two pore models is the arrangement of the bilayer: in the barrel-stave pore model, the hydrophilic part of the peptides point toward a water channel and the hydrophobic part toward the hydrophobic lipid side chains, whereas in the toroidal pore model the pore is formed by a complex of peptides and lipids aligning along an aqueous channel. Furthermore, AMPs can disrupt the membrane by a carpet-like mechanism [9,22,32,34] where the association of the peptides with the lipid head groups destabilizes the membrane and leads to a loss of membrane integrity. For the carpet-like model, no specific peptide-peptide interactions are required. The final collapse of the membrane bilayer structure into micelles is known as the detergent-like model [9].

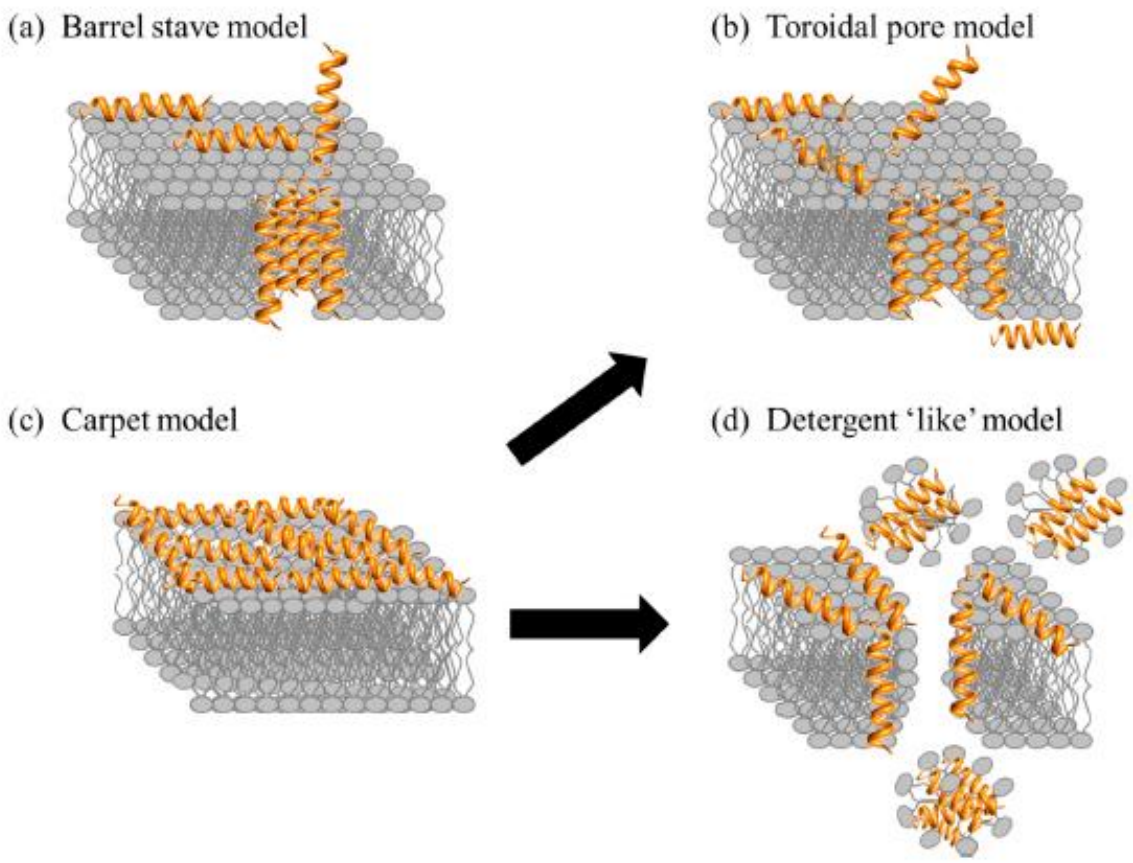

Figure 6. Models describing the interaction of antimicrobial peptides with membranes. (A) barrel stave model, (B) toroidal pore model, (C) carpet model, (D) detergent-like model [9].

In addition to the above described classical mechanisms further scenarios on a molecular level, described by Lohner, can occur and might interrelate to each other depending on the lipid's and peptide's nature. These mechanisms comprise interfacial activity, void formation, clustering of lipids and different effects on membrane curvature [33].

The interfacial activity model is based on the perturbation of the lipid packing of the membrane. The hydrophobic core is defined as the zone between the two bilayer interfacial zones acting as a permeability barrier for charged and polar molecules. Incorporation of a peptide in the hydrophobic core of the bilayer leads to a deformation of the bilayer and a disruption of the hydrogen chain packing, whereby the hydrophobic and charged groups of the peptide are accommodated. AMPs with unideal amphipathicity, like natural AMPs, are more prone for membrane perturbation than peptides that exhibit perfect segregation of hydrophobic and polar amino acids, as it applies to synthetic AMPs [33].

The free volume model describes the formation of a quasi-interdigitated gel phase leading to bilayer thinning. Ideally, amphipathic peptides may rather exhibit a parallel alignment to the membrane surface, leading to an energetically unfavorable free volume (void) formation in the bilayer. The prevention of the void leads to a quasi-interdigitated bilayer structure depending on the lipid composition of the membrane, that governs the peptide's penetration depth into the bilayer. In addition, AMPs penetrate more deeply in zwitterionic than in anionic bilayers [33].

Another model pictures the lateral lipid phase separation in bilayers induced by AMPs resulting in charge clustering. The resultant domains are laterally heterogeneous as the peptides are preferentially located in one domain. The domains display different thermotropic and structural behavior as well as diverse physicochemical properties like membrane thickness or curvature strain. These differences between the lipid domains enriched with peptides and the lipid bulk phase cause a reduction of the membrane permeability barrier since packing defects emerge at the boundary line of the lipid bulk phase and the lipid domains. These lipid clustering effects can deactivate membrane proteins that are essential for cell division or lead to perturbation of the lipid reorganization. Conformationally more flexible AMPs with sequences high in cationic residues will tend the most to perform this mechanism. According to Lohner [33], this mechanism is rather expected for Gram-negative bacteria [33].

Moreover, AMPs influence membrane curvature strain [33], that is initiated by the incorporation of these peptides in the bilayer. As described by Koller and Lohner, membrane curvature is triggered by high peptide concentrations and increased temperatures [35]. The major bacterial membrane lipids are PE and PG, whereby PE exhibits an inverted truncated cone shape. The molecular shape of PG is cylindrical [33]. By inserting a volume in the membrane interface and subsequently causing lateral pressure, AMPs can trigger induction of negative spontaneous curvature promoting the hexagonal phase in PE containing membranes. Otherwise, lateral pressure in the acyl chain region caused by an inserted volume in the hydrophobic core region facilitates positive spontaneous curvature by stabilizing the bilayer composed of PG [35]. Peptide binding and insertion into the membrane affects membrane curvature and vice versa. As the lateral hydrocarbon chain pressure is affected by AMPs, it may also lead to conformational changes of integral membrane proteins and have consequences on the membrane function [33].

Another novel mode of action which was recently described by Scheinpflug et al. is based on their work carried out with the antimicrobial peptide cWFW tested on *B. subtilis*. This mechanism comprises reduction of the membrane fluidity, membrane phase separation with subsequent influence on the membrane protein distribution, membrane protein delocalization, cell growth inhibition and cell wall autolysis. The membrane domains resulting from the reduced membrane fluidity that is initially caused by the AMP, trigger disruption of the membrane protein organization as the peripheral and integral proteins are segregated into domains displaying different rigidity. The peptide induced delocalization of the proteins affects the inhibition of cell wall synthesis and subsequently leads to cell lysis [36].

1.9. PHOSPHOLIPIDS AS MODEL MEMBRANE SYSTEMS

To study the interaction between peptides and the cell membrane, more specifically lipids, liposomes or lipid vesicles are useful model membrane systems that mimic the plasma membrane of bacteria. According to Malanovic et al., the study of pure lipids in detail is the basis for understanding the effects observed when antimicrobial peptides interact with the lipid matrix [3]. In this study, PG and CL were used in a molar ratio of 80:20 which nearly resembles the composition of the cytoplasmic membrane of *Enterococcus hirae*. The exact molecular structure of the lipids used in this study are shown in Figure 7. The physicochemical properties of PG and CL are presented in Table 1.

DMPG:TMCL = 80:20

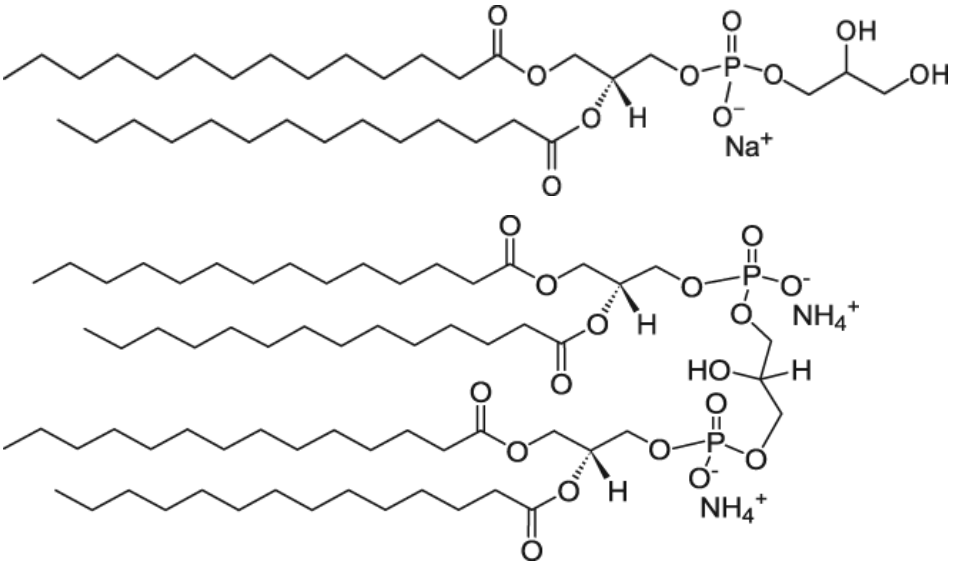

POPG:TOCL = 80:20

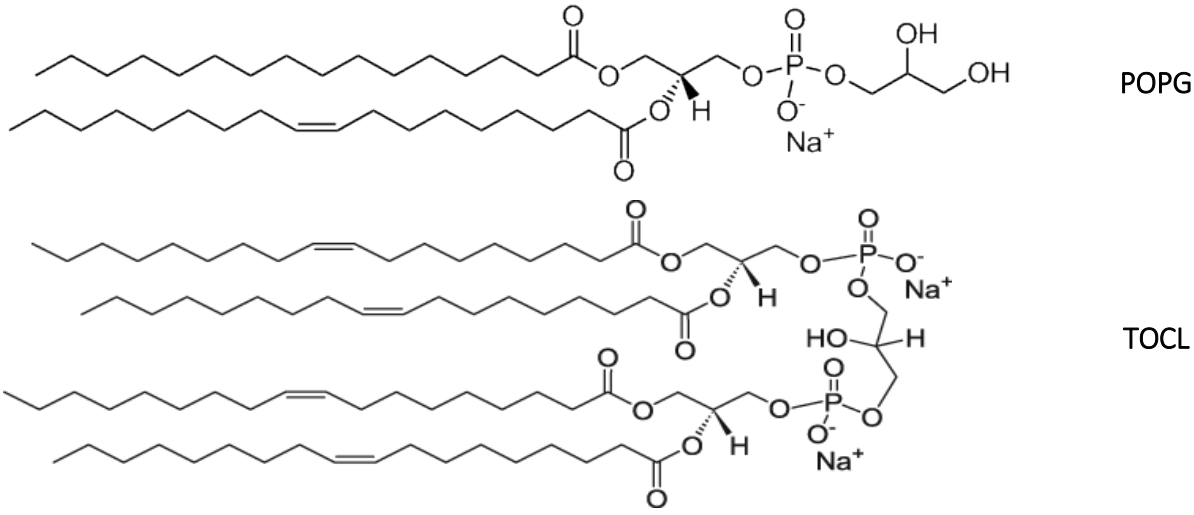

Figure 7. Phospholipid structure of DMPG, TMCL, POPG and TOCL, taken from Avanti Polar Lipids https://avantilipids.com/product-category/phospholipids/, accessed on 3 June 2019.

Table 1. Physicochemical properties of the Gram-positive bacterial phospholipids PG and CL, taken from [3]

	PG	CL
Net charge	-1	-2 (-1)
H-bonding ability	no	yes
Molecular shape	cylindrical	inverted truncated cone
Intrinsic curvature	zero	negative
Organization	bilayer	inverse micelles

1.10. WORKING MODEL

The working model of this thesis is that the antimicrobial peptides OP-145, SAAP-148, I12K exhibit antimicrobial activity against *Enterococcus hirae* based on a membrane-disruptive mechanism. Here, we investigated the mode of action of these AMPs. Different questions have been addressed to examine the peptides' interaction with bacterial membranes regarding, for instance, electrostatic interactions, membrane depolarization, membrane permeabilization and membrane fluidity. Biophysical studies have been accomplished in model systems and live bacteria. Furthermore, as all three peptides display different physicochemical properties in terms of net charge, total hydrophobicity and amphipathicity (molecular shape) [3], they show different killing potential. Therefore it was expected to observe differences in the mode of action between the peptides and the membrane. The outcome of this study will be helpful for the design of more potent AMPs.

2. EXPERIMENTAL PROCEDURES

2.1. MATERIALS

Unless otherwise indicated, all solutions were prepared in NaPi buffer pH 7.4, containing 20 mM NaPi and 130 mM NaCl. Sodium chloride and disodium phosphate waterfree were obtained from Carl Roth, disodium phosphate monohydrate from Merck. For leakage assays HEPES buffer pH 7.4 was used, composed of 10 mM HEPES and 140 mM NaCl. 4-(2-Hydroxyethyl) piperazine-1-ethanesulfonic acid (HEPES, ≥ 99.5%) was acquired from Sigma-Aldrich.

2.2. BACTERIAL STRAIN

Enterococcus hirae ATCC10541 was obtained from LGC Standards GmbH (Mercatorstr. 52, 46485 Wesel, Germany).

2.3. PHOSPHOLIPIDS

Phospholipids (>99% purity) 1-palmitoyl-2-oleoyl-sn-glycero-3-phospho-(1'-rac-glycerol) (POPG; MW = 770.99 g/mol), 1,2-dimyristoyl-sn-glycero-3-phospho-(1'-rac-glycerol) (DMPG; MW = 688.85 g/mol), 1',3'-bis[1,2-dioleoyl-sn-glycero-3-phospho]-glycerol (TOCL; MW = 1808.21 g/mol) and 1',3'-bis[1,2-dimyristoyl-sn-glycero-3-phospho]-glycerol (TMCL; MW = 1275.69 g/mol) were purchased from Avanti Polar Lipids (Alabaster, AL).

2.4. ANTIMICROBIAL PEPTIDES

The peptides OP-145, SAAP-148 and I12K, which were used in this study are represented in Figure 3. They were synthesized by our collaborator Jan Wouter Drijfhout (LUMC, Leiden, The Netherlands). Purity of the peptides was >95%.

2.5. METHODS

2.5.1. GROWING CONDITIONS OF THE BACTERIAL STRAIN *ENTEROCOCCUS HIRAE*

For overnight culture Brain-Heart-Infusion Broth (BHIB) (Carl Roth; Beef heart 5 g/l, calf brains 12.5 g/l, disodium hydrogen phosphate 2.5 g/l, D(+)-glucose 2g/l, peptone 10 g/l, sodium chloride 5 g/l, final pH 7.4±0.2 (25°C)) was inoculated with *E. hirae* cells of a single colony placed at 37°C under shaking conditions overnight. After that, the main culture was inoculated starting by OD=0.01 and incubated in fresh BHIB medium to midlogarithmic phase for 3 h 30 at 37°C by shaking (OD is approximately 1).

2.5.2. PREPARATION OF LIPOSOMES

The preparation of lipid films has been performed by using an appropriate amount of phospholipid solved in chloroform/methanol (9:1 v/v) (Carl Roth), followed by evaporation under a stream of nitrogen for 30 minutes at 35 °C and storage in vacuum overnight. After addition of NaPi buffer or fluorophore-buffer in case of leakage assay formation of lipid vesicles was achieved by intermittent vigorous vortexing at 65°C. For Zeta-potential measurements or leakage assays, large unilamellar vesicles (LUV) were obtained by extrusion of multilamellar vesicles through a polycarbonate filter (Millipore-Isopore™) of 0.1 µm pore size. Vesicle size has been measured using the Zetasizer Nano (ZSP, Malvern. For lipid mixture, the appropriate amount of phospholipid can be calculated according to:

$$mA\ [mg] = \frac{mol\ \% * mA}{mol\ \% * mA + mol\ \% * mB}$$

where mA denotes the molecular weight of lipid A, mB the molecular weight of lipid B, $mol\ \%$ is the molecular percentage of one phospholipid in the mixture [2].

2.5.3. ANTIMICORBIAL ACTIVITY OF OP-145, SAAP-148, I12K

After culturing the cells in BHIB, they were washed once with NaPi buffer. $1x10^6$-$1x10^9$CFU/ml *E. hirae* in NaPi buffer were incubated for 15 minutes with the defined peptide concentration. Antimicrobial activity can be determined by plating 100 µl sample on diagnostic sensitivity Brain-Heart-Infusion agar (BHIB + 2 w% agar (Carl Roth GmbH + Co. KG)) and subsequent

establishing of the number of viable bacteria after incubation at 37°C overnight. The 99.9% lethal concentration ($LC_{99.9\%}$) implies antimicrobial activity and constitutes the lowest peptide concentration that killed ≥ 99.9% of bacteria [2].

2.5.4. DEPOLARIZATION ASSAY ON *ENTEROCOCCUS HIRAE*

Membrane depolarization was performed by using *E. hirae* cells in mid-logarithmic phase, which were collected by centrifugation, washed twice and then resuspended in NaPi buffer to an OD of 0.0125 ($1x10^7$ CFU/ml). To investigate the cytoplasmic membrane depolarization by OP-145, SAAP-148 and I12K 1 µM cyanine dye $DiSC_3$ were applied. To allow dye uptake, the cells were incubated for 30 minutes in the dark. Before the measurement, 100 mM KCl were added. The desired AMP was added gradually to yield a final concentration of 51.2 µM peptide. 3.5 µM Melittin (Sigma-Aldrich) and 1 % Triton 100 (Carl Roth) acted as positive control. The fluorescence reading was recorded by using a VARIAN Cary Eclipse Fluorescence Spectrophotometer at an excitation wavelength of 622 nm and an emission wavelength of 685 nm with a slit width of 5 nm. High precision QS-cuvettes (10x10 mm) from Helma Analytics were used for all measurements with a volume of 2 ml [36].

2.5.5. FLUORESCENCE SPECTROSCOPY AND LEAKAGE ASSAY ON LIPOSOMES

Leakage of the aqueous content from large unilamellar vesicles (LUVs) composed of POPG and POPG/TOCL upon incubation with peptide was determined by using 20 mg/ml lipid vesicles of defined size loaded with 8-aminonaphthalene-1,3,6,-trisulfonic acid/*p*-xylene-bis-pyridinium bromide (ANTS/DPX). Separation of the LUVs from the free fluorescent dye was performed by exclusion chromatography using a column filled with Sephadex™ G-75 (Amersham Biosciences) fine gel swollen in an iso-osmotic buffer (19 mM HEPES, 140 mM NaCl, pH 7.4). The phospholipid concentration determination was carried out, as described in Chapter 2.5.6. (phosphate determination). Fluorescence emission spectra were obtained using an excitation wavelength of 360 nm, an emission wavelength of 530 nm and a slit width of 10 nm. The fluorescence measurements were performed in quartz cuvettes (10x10 mm, high precision cell, Helma Analytics) with an initial lipid concentration of 50 µM in 2 ml HEPES buffer. Fluorescence emission was recorded as a function of time before and after the addition of gradual amounts

of the peptide. Because of leakage and subsequent dilution of dye, the observed fluorescence increase was measured after peptide addition ranging from 0.25 up to 8 µM. The measurements were carried out on a VARIAN Cary Eclipse Fluorescence Spectrophotometer combined with Cary Eclipse Software. Percentage of leakage was calculated from the fraction

of the leakage (I_F) according to: $$I_F = \frac{(F-F_0)}{(F_{max}-F_0)}$$

where F is the measured fluorescence, F_0 is the initial fluorescence without peptide and F_{max} is the fluorescence corresponding to 100% leakage achieved by the addition of 1% Triton X-100 [2,37].

2.5.6. PHOSPHATE DETERMINATION

To determine the phosphate content in the LUVs (20 mg/ml) for subsequent fluorescence measurement, the standard protocol authored by Broekhuyse (1986) was taken as a basis. The lipid samples were heated first for about 1 minute at 180°C in an electrically heated metal block. To each tube 0.4 ml acid mixture (conc. H_2SO_4:$HClO_4$ = 9:1) was added and heated for further 30 minutes at 180°C. After cooling 9.6 ml of a mixture (22 ml reagent A: 10.5 mM ANSA (1-amino-2-hydroxy-naphthalin-4-sulfonic acid), 0.7 mM $Na_2S_2O_5$, 40 mM Na_2SO_3; 500 ml reagent B: ammonium heptamolybdate tetrahydrate (0.26 %)) was added. After mixing the tubes were placed in a sand bath at 90°C for 20 minutes. The extinction of the cooled samples was measured on a Spectrophotometer Onda V-10 Plus at 830 nm. The phospholipid concentration was calculated by using the calibration curve (3.2 mM KH_2PO_4 as phosphate-standard-solution containing 1 - 14 µg phosphor). H_2SO_4 (96 % v/v), $Na_2S_2O_5$ and Na_2SO_3 were purchased from Carl Roth, $HClO_4$ and ammonium heptamolybdate tetrahydrate (2.60 g/l) from Sigma-Aldrich and ANSA and KH_2PO_4 (0.0997 mg/ml) from Merck.

2.5.7. ZETA-POTENTIAL MEASUREMENTS OF LIPOSOMES AND *ENTEROCOCCUS HIRAE*

Zeta-potential measurements were carried out on a Zetasizer Nano (ZSP, Malvern) using disposable folded polycarbonate capillary cells (Malvern). HEPES buffer was filtered by using a syringe filter with 0.02 µm pore size (AnotopTM). Concerning the membrane model system, 50 µM LUVs were mixed with the appropriate peptide amount that varied from 0.125 to 8 µM.

Regarding live bacteria, $1x10^7$ CFU/ml cells were measured with 0.8 – 51.2 µM of the appropriate peptide [38,39].

2.5.8. MEMBRANE PERMEABILIZATION OF *ENTEROCOCCUS HIRAE* BY FLOW CYTOMETRY

After following the instructions from Chapter 2.5.1. (growing conditions of the bacterial strain *Enterococcus hirae*) the cells were washed with NaPi buffer twice (5 min, 5100 g), diluted to $1x10^6$ CFU/ml with NaPi and stored on ice. 600 – 1200 µl of the cell suspension were incubated with propidium iodide (PI, 1 µg/ml final concentration) followed by the fluorescence measurement in polystyrene tubes with the flow cytometer BD LSR Fortessa™ using the BD FACSDiva Software (excitation: 488 nm, emission: 695/40 nm, PerCP-Cy5.5 channel). To distinguish between PI-positive and PI-negative cell populations, selective gating was used. The scan rate was at 300 – 400 events per second. After 30 seconds the appropriate peptide amount has been added to the labeled bacterial cells, followed by the fluorescence measurement for 10 minutes for OP-145 and SAAP-148 treated cells, 20 minutes for I12K. For the analysis of PI-positive cells, the fcs-files from the BD FACSDiva Software had to be extracted into csv-files by using FCSExtract Utility (version 1.02). The percentage of PI-positive cells was calculated at different time intervals in Microsoft Excel.

2.5.9. FLUORESCENCE MICROSCOPY OF *ENTEROCOCCUS HIRAE*

E. hirae strains were prepared as described in Chapter 2.5.1. (growing conditions of the bacterial strain *Enterococcus hirae*), washed with NaPi buffer twice (5 min, 5100 g) and diluted to $2.5x10^8$ CFU/ml. The incubation of the cells with the appropriate peptide concentration was accomplished for about 10 minutes and followed by the addition of the fluorescent membrane dye Nile Red (10 µg/ml, Sigma Aldrich). One minute later the cells were centrifuged and 2 µl of the pellet was put on a microscope slide with agar (2 w%; 50 ml of 2 % agar (Sigma, Inc.) melted at 600 W, for 5 min) covered with a coverslip of 0.17 µm thickness (Menzel, Inc.). Microscopy was performed by using a Leica SP5 confocal microscope (Leica Microsystems, Inc.) with spectral detection and a Leica HCX PL APO CS 63x NA 1.4 oil immersion objective. The excitation wavelength of Nile Red was at 561 nm. Fluorescence emission detection ranged from 570 to 750 nm. 47x47 nm sampling (x/y) were used for image recording.

2.5.10. DIFFERENTIAL SCANNING CALORIMETRY (DSC) ON LIPOSOMES

DSC measurements were performed using a Nano-DSC high sensitivity differential scanning calorimeter (Waters). Scans of 1 mg/ml lipid concentration were recorded at a constant rate of 0.5°C/min. Data were analyzed using Launch NanoAnalyze. After normalization to the mass of phospholipid and baseline correction, the calorimetric enthalpies were calculated by the integration of the peak areas. The temperature at the peak maximum indicates the phase transition temperature.

3. RESULTS

3.1. ANTIMICROBIAL ACTIVITY OF OP-145, SAAP-148 AND I12K

For determining the lethal peptide concentration ($LC_{99.9\%}$) of SAAP-148, OP-145 and I12K on *Enterococcus hirae,* a killing assay was performed by examining antimicrobial activity of the peptides as previously reported in Chapter 2.5.3.. Each peptide was tested three times at different times ranging from 5 to 120 minutes. The averaged results are presented in Table 2.

Table 2. Antimicrobial activity of SAAP-148, OP-145 and I12K against *E. hirae*. $1x10^6$ CFU/ml of *E. hirae* were exposed to 0.1-0.4 µM of SAAP-148, 0.8-3.2 µM of OP-145 and 25.6-102.4 µM of I12K. After 5, 10, 20, 30, 60, and 120 minutes of incubation, the numbers of viable bacteria were determined by counting the CFUs. Lethal concentrations ($LC_{99.9\%}$) are indicated in the table. Data are the summary of three independent experiments.

Peptide	Concentration (µM)	Time (min)					
		5	10	20	30	60	120
SAAP-148	0.1		$LC_{99.9\%}$				
	0.2		$LC_{99.9\%}$				
	0.4	$LC_{99.9\%}$					
OP-145	0.8					$LC_{99.9\%}$	
	1.6		$LC_{99.9\%}$				
	3.2	$LC_{99.9\%}$					
I12K	25.6						$LC_{99.9\%}$
	51.2				$LC_{99.9\%}$		
	102.4			$LC_{99.9\%}$			

SAAP-148 is the peptide with the highest cytotoxic activity regarding killing *E. hirae*. Its killing concentration is at 0.1 and 0.2 µM after 10 minutes. After 5 minutes, the lethal concentration $LC_{99.9\%}$ of SAAP-148 is at 0.4 µM. OP-145 is lethal against *E. hirae* within 5 minutes at a concentration of 3.2 µM. After 10 minutes of incubation 1.6 µM OP-145 cause killing of *E. hirae*, 0.8 µM OP-145 after 60 minutes. Referring to experimental data I12K is the peptide with least

antimicrobial activity. The $LC_{99.9\%}$ is reached after 120 minutes at 25.6 µM, after 30 minutes at 51.2 µM and after 20 minutes at 102.4 µM.

3.2. EFFECTS ON MEMBRANE INTEGRITIY OF LIVING *E. HIRAE* CELLS

Changes of *E. hirae* cells' membrane integrity were observed by performing Zeta-potential measurements, determining membrane depolarization and examining membrane permeability and fluidity.

3.2.1. EFFECTS ON THE CELL SURFACE CHARGE

In order to assess surface charge neutralization of Gram-positive *E. hirae*, Zeta-potential measurements were performed using SAAP-148, OP-145 and I12K.

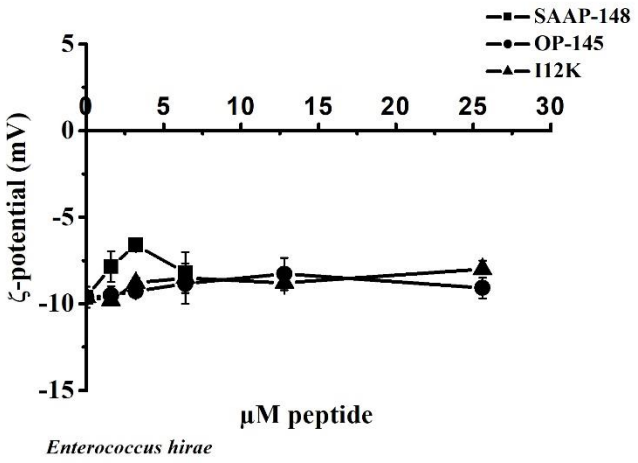

Figure 8. Effect of SAAP-148, OP-145 and I12K on *E. hirae* cells. Zeta-Potential measurements of *E. hirae* in absence and presence of SAAP-148 (squares), OP-145 (circles) and I12K (triangles) at indicated concentrations ranging from 0.8 to 25.6 µM. Data are the summary of three independent experiments.

No neutralization of the membrane surface charge is detectable, indicating that all three peptides can reach the membrane without significantly interacting with the cell wall components. No big difference between the three peptides is observed (Figure 8).

3.2.2. DEPOLARIZATION OF THE INNER MEMRANE

For examining membrane depolarization of *E. hirae,* a depolarization assay was performed. Peptide-induced changes in the membrane potential of the bacterial cells were measured using the voltage-sensitive fluorescent dye $DiSC_3(5)$. $DiSC_3(5)$ is a cationic dye that translocates into the inner membrane via self-association in the hydrophobic environment and remains there as

an oligomer. If the membrane becomes disrupted, the dye will be released. Melittin (3.5 µM) acts as the positive control and indicates 100% membrane depolarization.

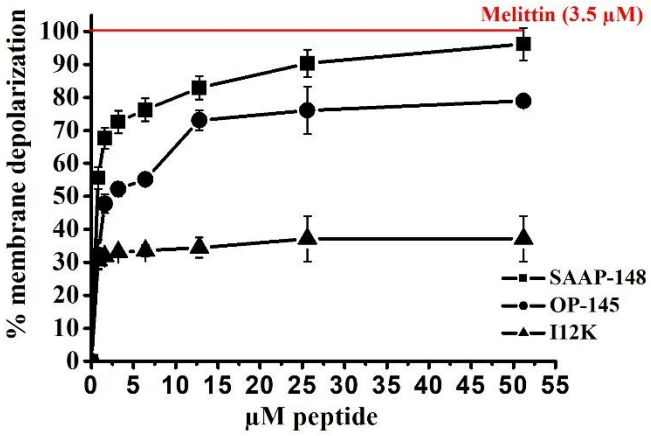

Figure 9. Effect of SAAP-148, OP-145 and I12K on *E. hirae* cells. Membrane depolarization of *E. hirae* at indicated peptide concentrations (SAAP-148 (squares), OP-145 (circles), I12K (triangles)) in the range of 0.8 to 51.2 µM. Red line represents full membrane depolarization. Data are the summary of three independent experiments.

As shown in Figure 9, the increase of the fluorescence intensity of $DiSC_3$-stained cell suspension leads to an increase of membrane depolarization concerning all three peptides, whereby SAAP-148 nearly reaches 100% at 51.2 µM. At the same concentration, OP-145 only achieves 80% of membrane depolarization. Comparing this data to the antimicrobial activity of SAAP-148, OP-145 and I12K against *E. hirae* (Table 2) full membrane depolarization is obviously no prerequisite for OP-145 and SAAP-148 to kill *E. hirae* as the lethal concentration is below 5 µM for both peptides. The fluorescence intensity of I12K treated cells increased only slightly, up to 30% at 51.2 µM of I12K.

3.2.3. MEMBRANE PERMEABILITY

The permeabilization of the plasma membrane by OP-145, SAAP-148 and I12K was tested in live bacteria using flow cytometric analysis of propidium iodide (PI) influx. In case of a cell membrane damage by AMPs the membrane impermeable PI can penetrate through the cytosol resulting in a fluorescence change and detection of PI-positive cells.

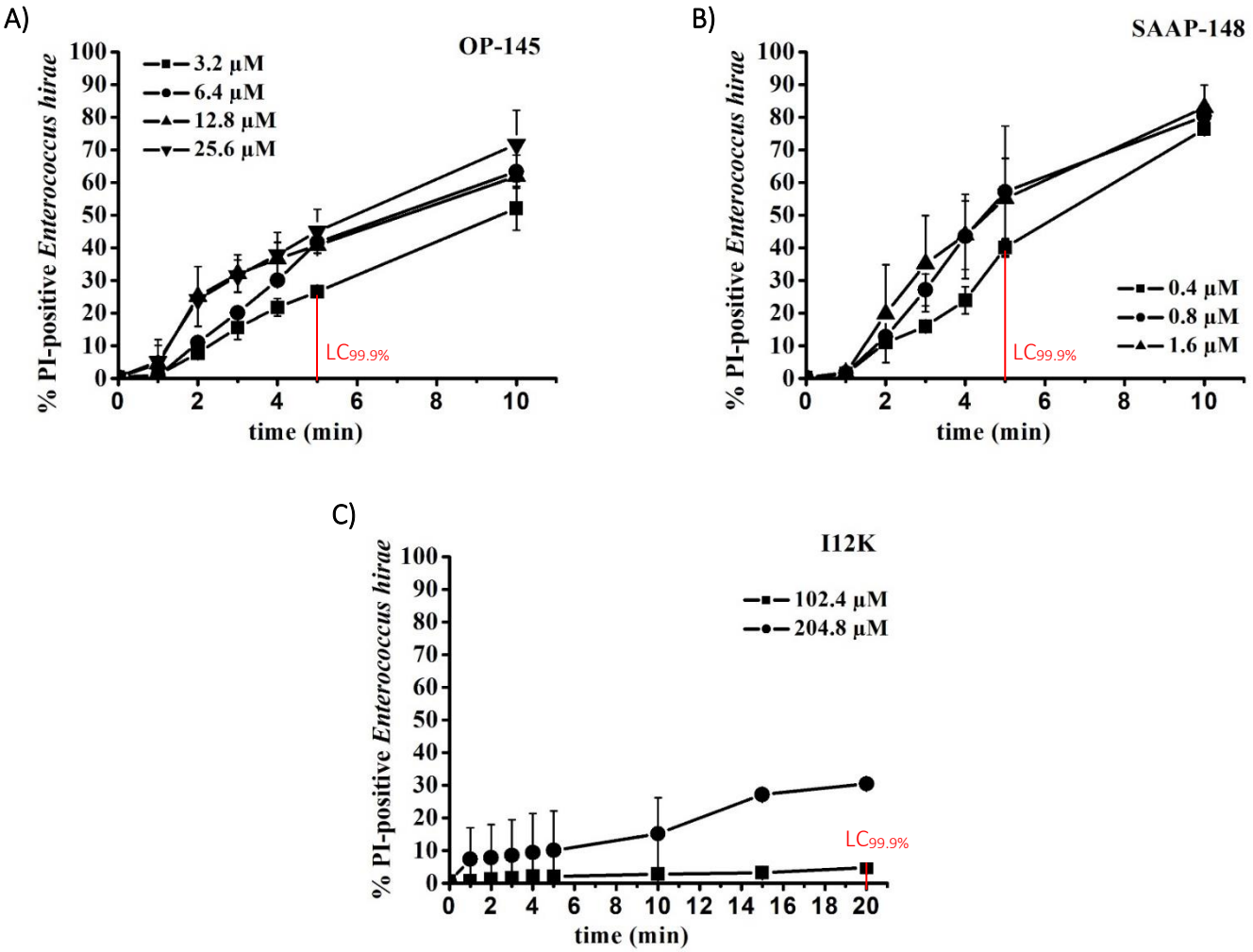

Figure 10. Membrane permeabilization of *E. hirae* by the peptides (A) OP-145, (B) SAAP-148 and (C) I12K. The percentage of PI-positive *E. hirae* cells was calculated at different time intervals after addition of 3.2 to 25.6 µM OP-145, 0.4 to 1.6 µM SAAP-148 and 102.4 to 204.8 µM I12K. Results are medians of three independent experiments. Lethal concentrations are indicated by red lines.

All three peptides dose-dependently permeabilize the membrane of *E. hirae* in a time-dependent manner. 25.6 µM OP-145 caused 72% permeabilization after 10 minutes. At the killing concentration of 3.2 µM after 5 minutes, only 27% of PI-positive cells are detectable. Within 10 minutes after exposure to 1.6 µM of SAAP-148, 83% of the *E. hirae* cells were permeabilized. The $LC_{99.9\%}$ of SAAP-148 is at 0.4 µM as marked in Figure 10B. However, after 5 minutes of incubation, only 40% of the cells are PI-positive. 204.8 µM I12K induces permeabilization in 30% of cells after 20 minutes. At the killing concentration of 102.4 µM and 20 minutes after exposure, only about 5% PI-positive *E. hirae* cells can be detected. These data of all three AMPs, OP-145, SAAP-148 and I12K, indicate that full membrane permeabilization is no requirement for killing bacteria.

3.2.4. MEMBRANE FLUIDITY

Membrane fluidity measurements were performed with fluorescence microscopy. Peptide-induced changes of the membrane fluidity of *E. hirae* were visualized with the fluorescent membrane dye Nile Red. This was achieved with E. *hirae* cells cultivated to mid-logarithmic phase and adjusted to OD_{600} of 0.2 in BHIB medium.

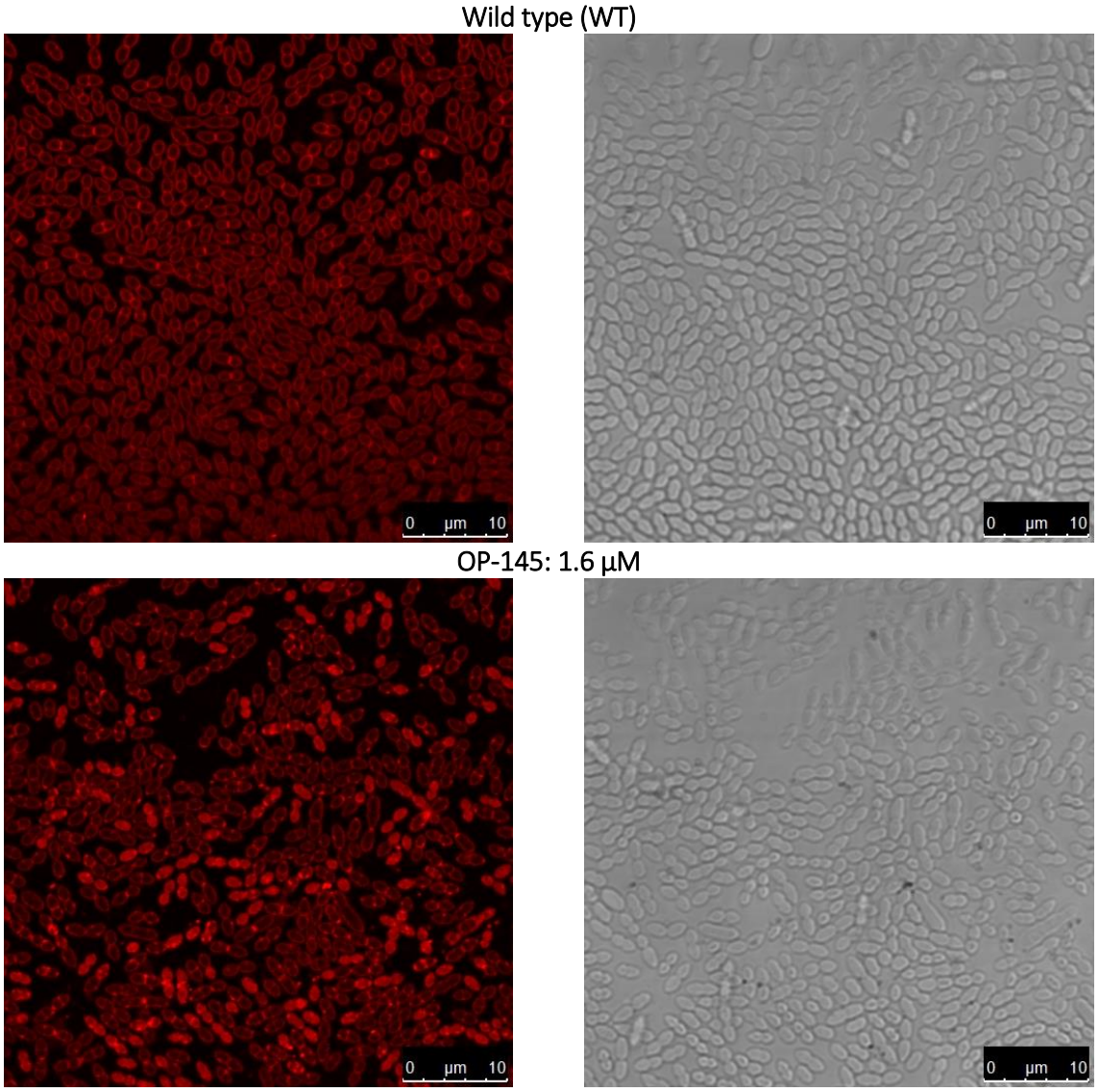

OP-145: 6.4 µM

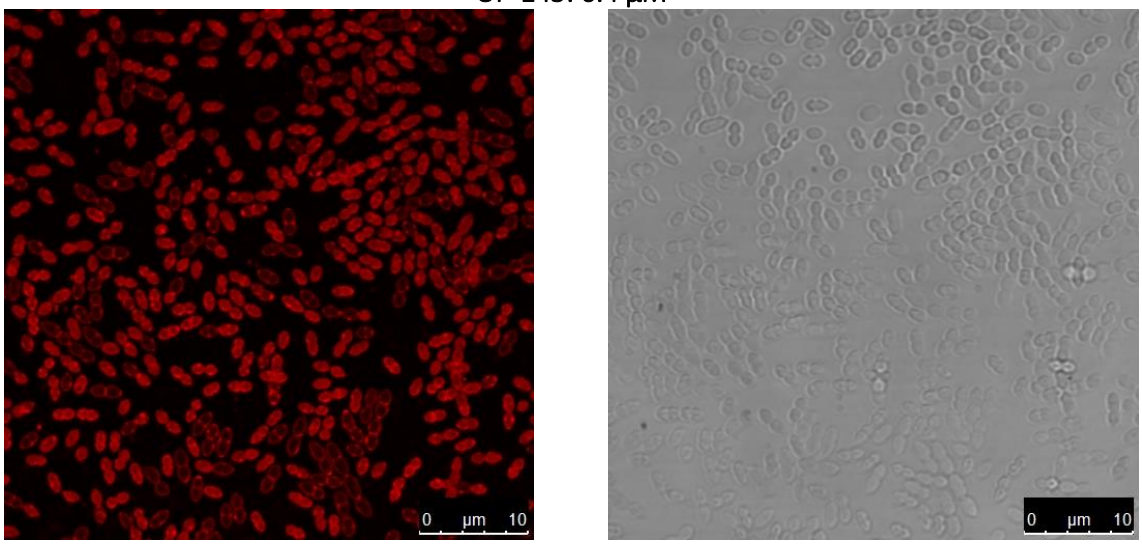

OP-145: 25.6 µM

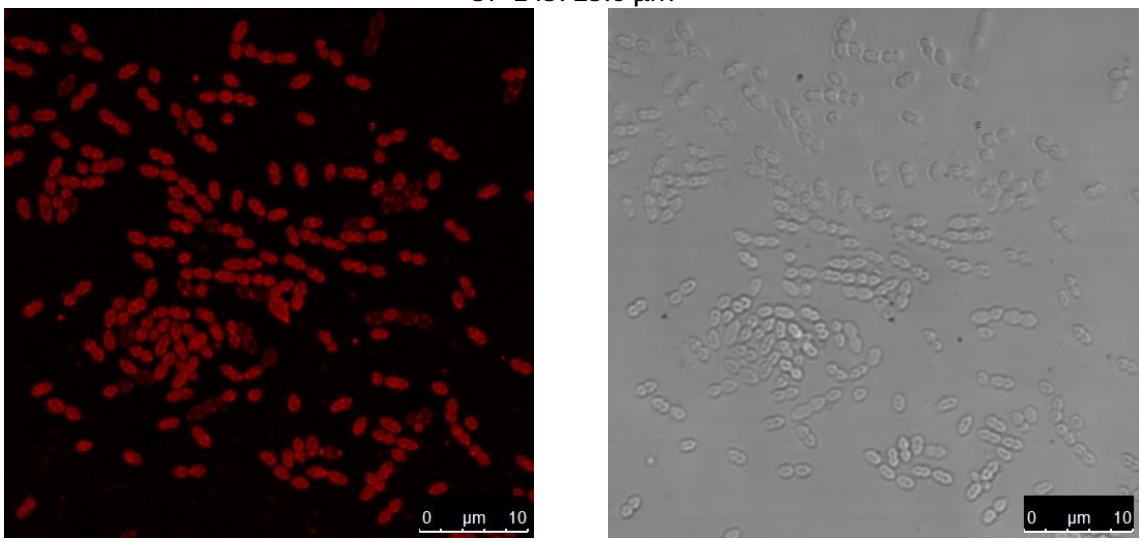

SAAP-148: 0.2 µM

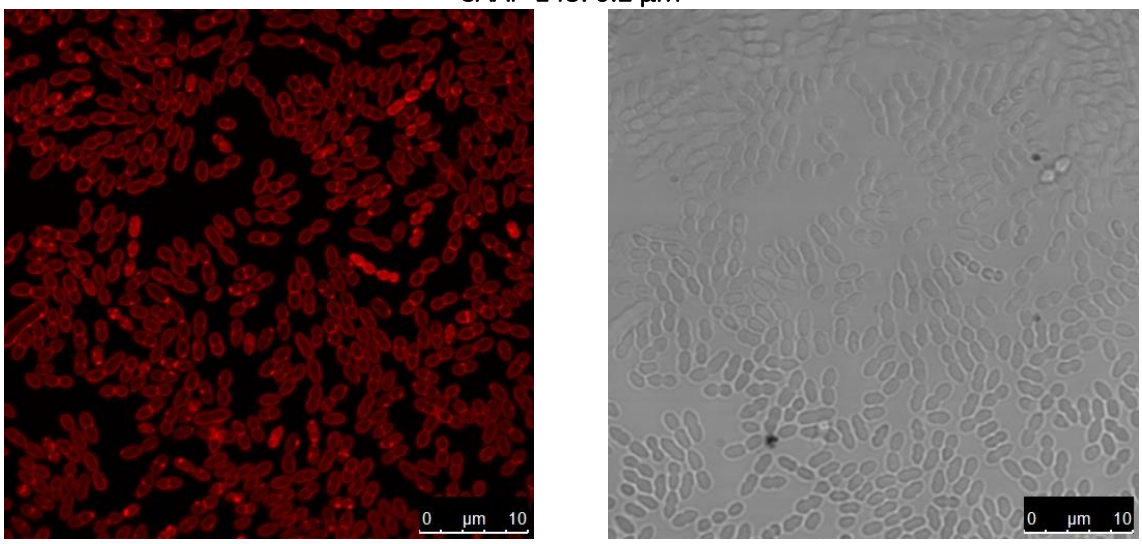

SAAP-148: 0.8 µM

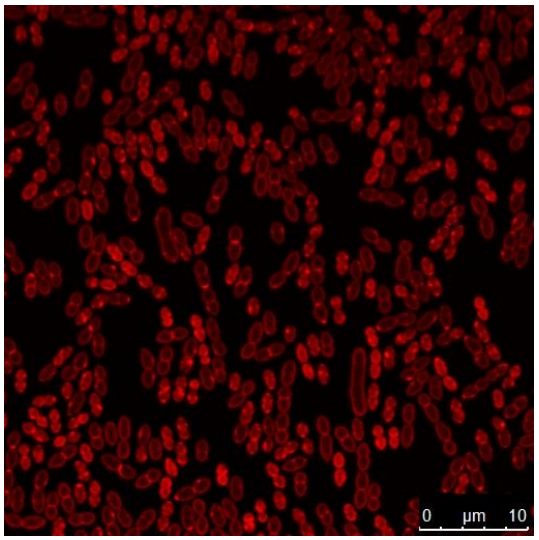

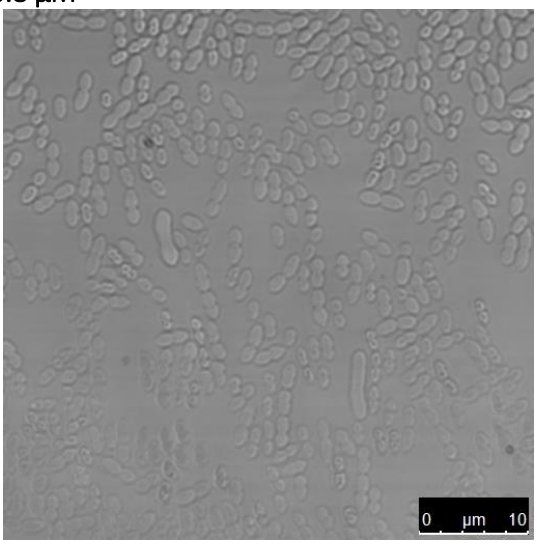

SAAP-148: 1.6 µM

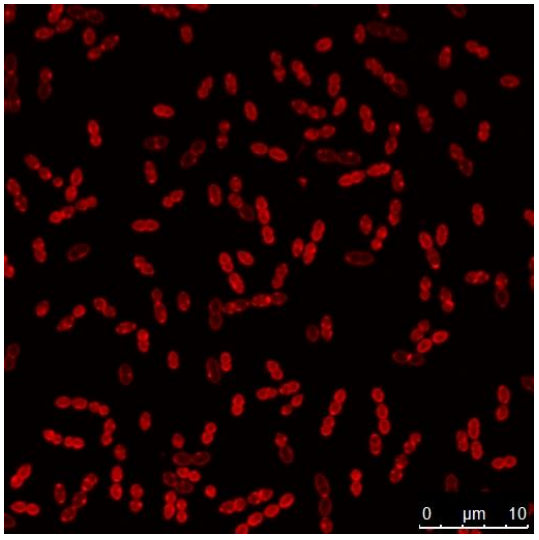

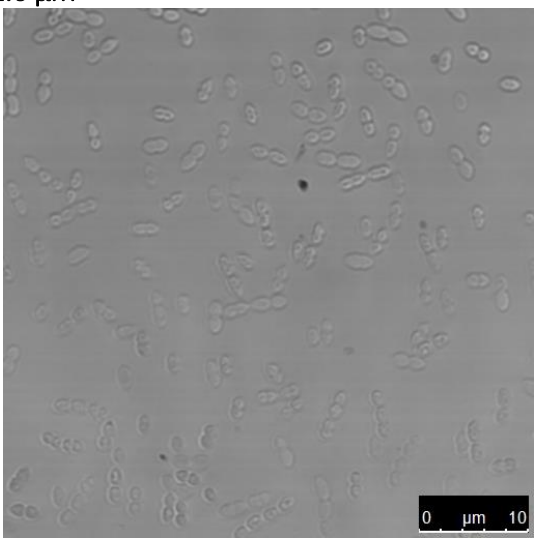

SAAP-148: 3.2 µM

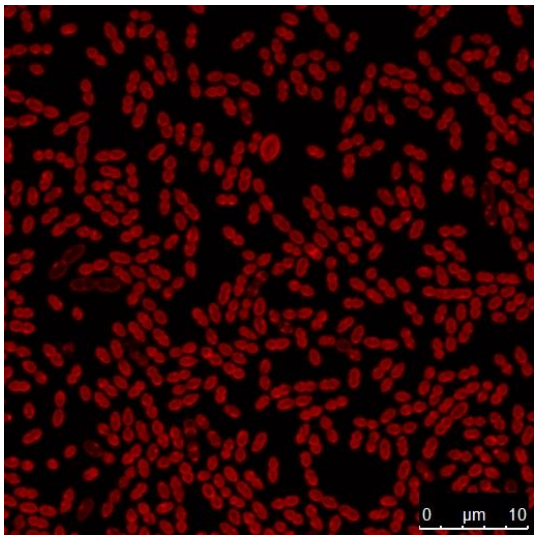

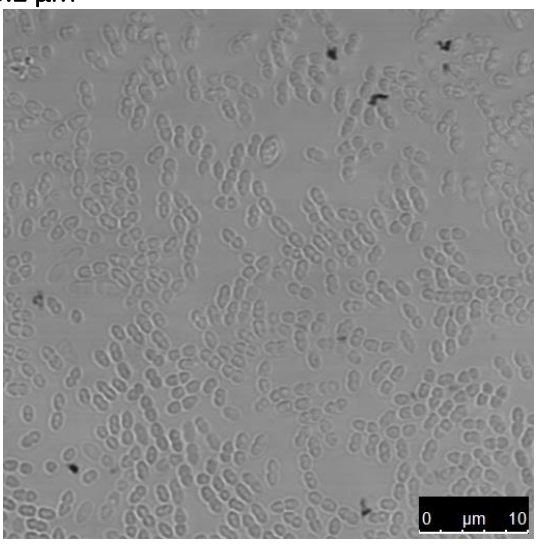

SAAP-148: 6.4 µM

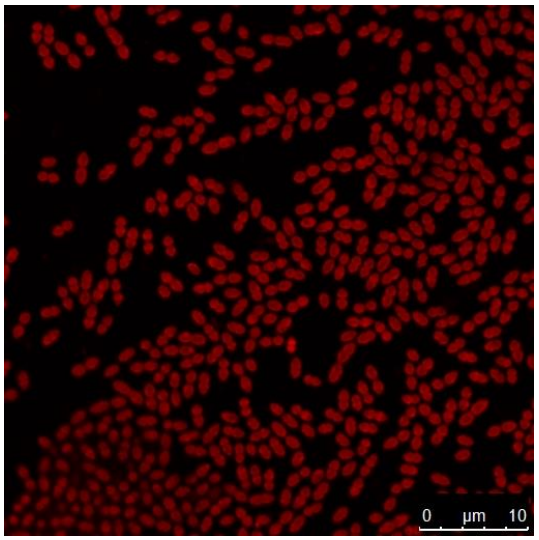

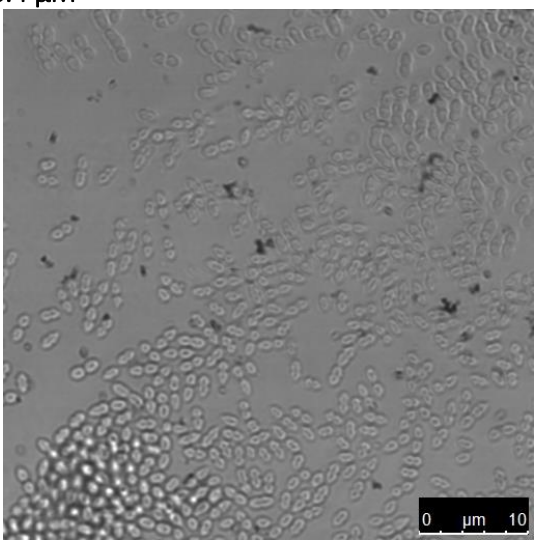

I12K: 12.8 µM

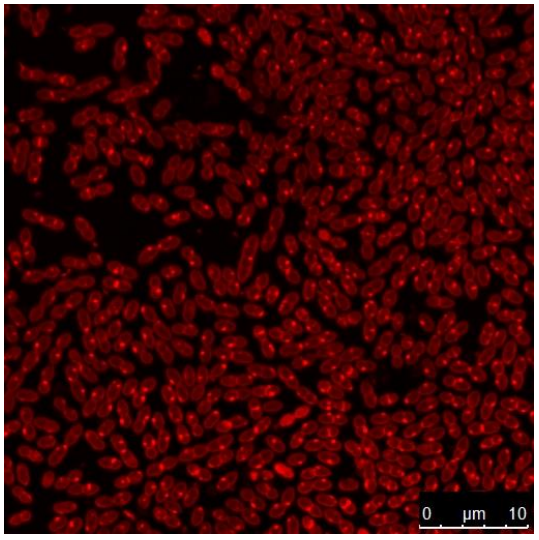

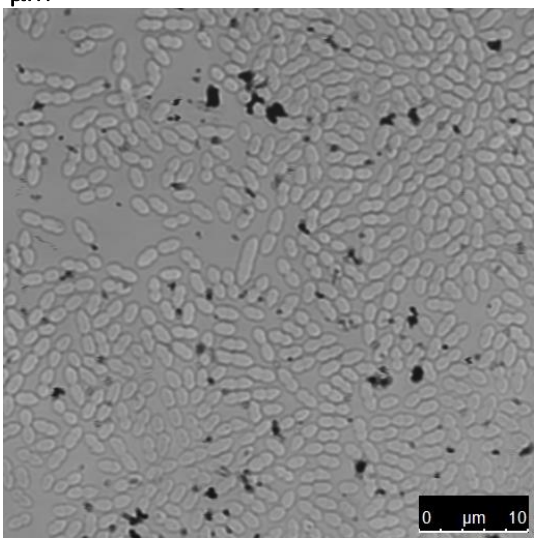

I12K: 51.2 µM

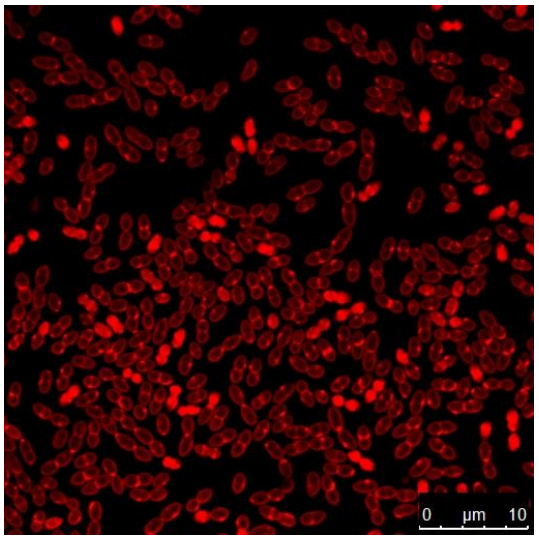

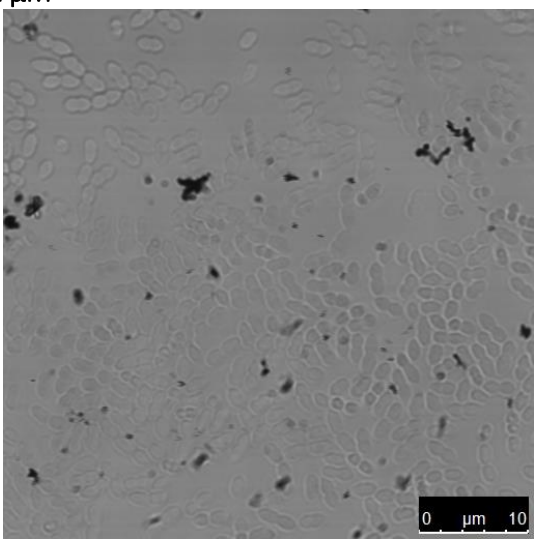

I12K: 102.4 µM

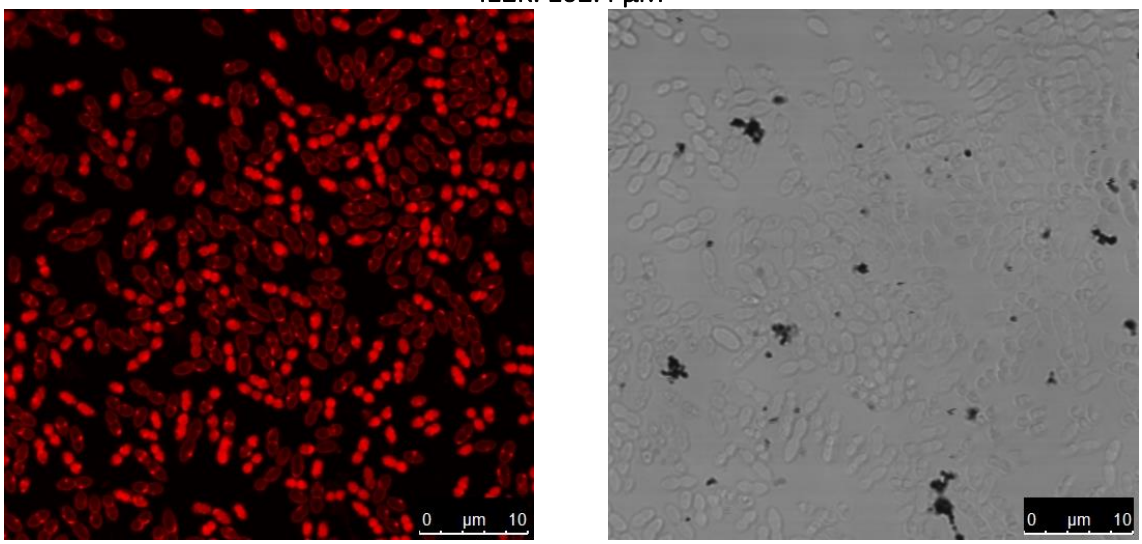

Figure 11. Fluorescence images of *E. hirae* cells stained with Nile Red untreated and after incubation with 1.6 - 25.6 µM OP-145, 0.8 - 6.4 µM SAAP-148 and 12.8 - 102.4 µM I12K. Pictures by bright field microscopy are represented on the right side.

Nile Red staining of untreated wildtype cells results in homogenous incorporation of the dye across the cell membrane. As *E. hirae* is a diplococci bacterium, intensively stained areas around the connection zones of two cocci are observed. Since the microscopic pictures are taken from mid-logarithmic growing cells, it can also not be excluded that the septum of the dividing cells [26] is stained.

The presence of all three peptides influences membrane staining, whereas each peptide's impact on *E. hirae* is pronounced differently. One characteristic all three peptides have in common is the appearance of a big Nile Red dot localized at either one or both septal poles of the cell. In some cases, these dots appear elsewhere in the membrane. The increase of the peptide concentration triggers the rise of the dot quantity. One peculiarity is that the number of domains per cell never exceed two, in some rare cases three. This, in turn, may be an indication for pore-forming mechanisms [9] of the peptides as the peptides do not accumulate on the entire membrane but rather show dots at specific membrane areas. In addition, all three peptides lead to a decrease in size of the cells. For OP-145-treated cells, perturbation of membrane fluidity rises with increasing peptide concentration. At the highest OP-145 concentration of 25.6 µM membrane fluidity of almost every cell is disturbed. SAAP-148 displays the same trend as OP-145. Increasing the lowest peptide concentration of 0.2 µM SAAP-148 with impact on dot formation in the cell membrane to 6.4 µM leads to a trigger of

dysfunctional membrane integrity. SAAP-148-treated cells shrink faster and even at a lower concentration compared to OP-145-treated cells. The main difference between I12K and the two other peptides is the homogenous intensively stained Nile Red dot distribution over the bacterial membrane, which is not exhibited by OP-145 and SAAP-148, where the dot appearance starts at low peptide concentrations at the poles and is localized in additional membrane areas at higher peptide concentrations. The disturbance of the fluidity is not that much pronounced for I12K. Despite the high I12K concentration of 102.4 µM, it does not lead to such a strong decrease in cell size like SAAP-148. The diameter of WT cells is about 2 µm, SAAP-148 shrinks the cells at the highest applied concentration of 6.4 µM to 0.98 µm, OP-145 (25.6 µM) does this up to a diameter of 1.5 µm and I12K (102.4 µM) up to 1.4 µm.

3.3. INTERACTION WITH MEMBRANE MIMICS

The plasma membrane of the Gram-positive bacterial strain *E. hirae* is almost solely composed of PG and a minor amount of CL (Malanovic et al. unpublished), which can increase during growth to the stationary phase [40]. To gain further information on lipid-specific interactions of OP-145, SAAP-148 and I12K, model membrane systems composed of POPG and POPG/TOCL (80:20) were used. Furthermore, membranes consisting of DMPG/TMCL (80:20) were used to elucidate the effect of saturation of the acyl chains on peptide interactions. For leakage experiments, the use of latter membranes was not suitable due to an instability of the vesicles. The impact of the peptides on surface charge and thermotropic behavior and their disruption capability of the respective model membrane were assessed by Zeta-potential measurements, DSC techniques as well as leakage assays.

3.3.1. EFFECTS ON THE SURFACE CHARGE NEUTRALIZATION

In addition to surface charge neutralization as determined for live cells (Chapter 3.2.1.), Zeta-potential measurements were performed on three different membrane models – POPG, POPG/TOCL as well as DMPG/TMCL in presence and absence of SAAP-148, OP-145 and I12K. In general, the Zeta-potential is the electric potential of a particle in an aqueous medium that exists at the slipping plane surrounding the Stern layer, which in turn covers the particle [39].

Figure 12. Effect of SAAP-148, OP-145 and I12K on bacterial membrane mimics. Zeta-Potential measurements of POPG in absence and presence of SAAP-148 (squares), OP-145 (circles) and I12K (triangles) at indicated concentrations ranging from 0.5 to 8 µM. Data are the summary of three independent experiments.

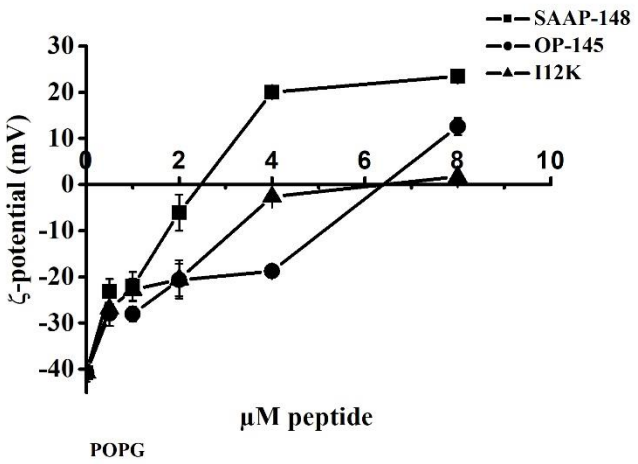

Addition of about 2 µM SAAP-148 alters the Zeta-potential of POPG liposomes almost toward a neutral threshold. Concerning the other peptides, the membrane model POPG shows surface charge neutralization at higher peptide concentrations (6 µM for OP-145 and 8 µM for I12K). Higher concentrations of SAAP-148 result in an overcompensation of the surface charge, which is not the case for the other two peptides.

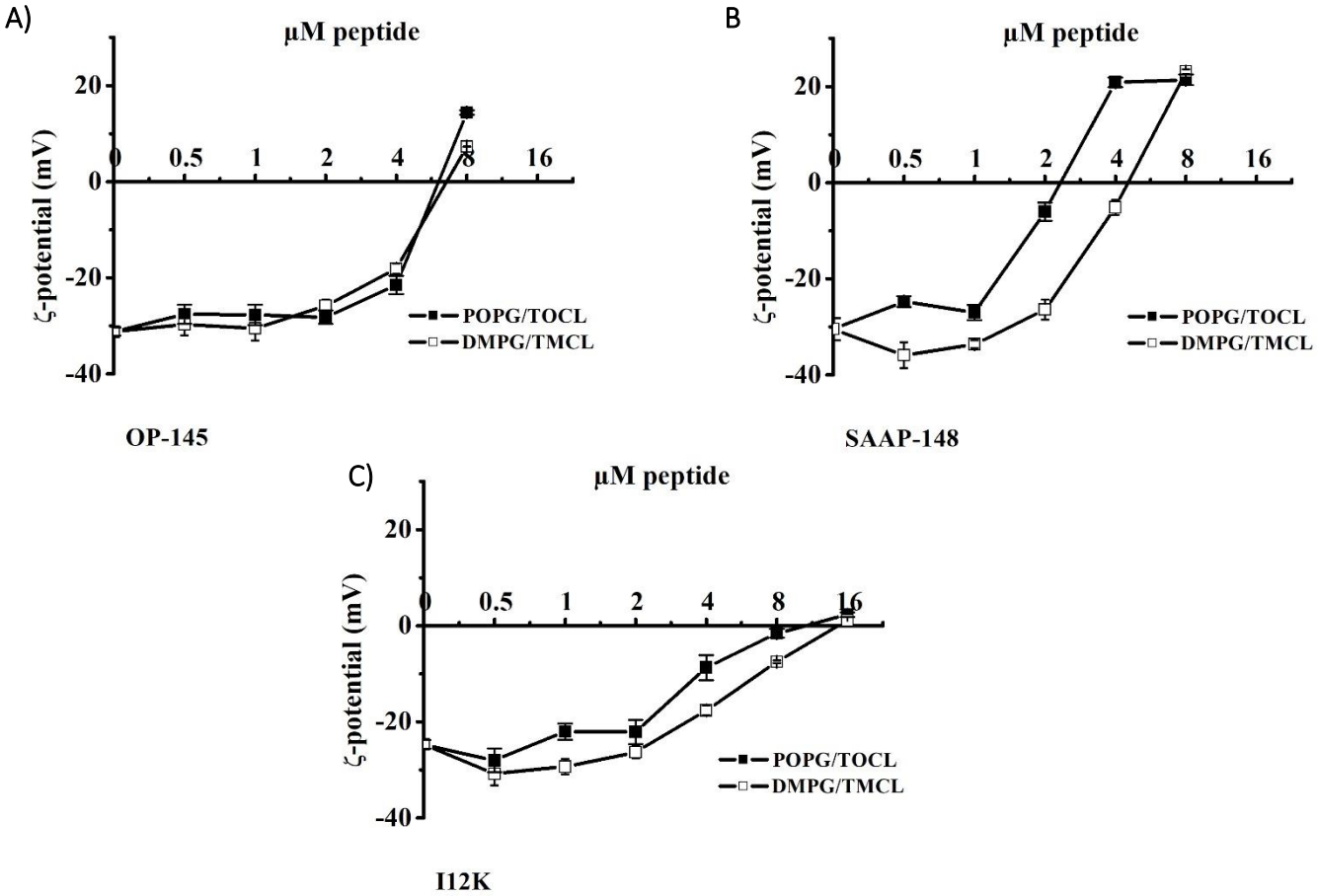

Figure 13. Effect of SAAP-148, OP-145 and I12K on bacterial membrane mimics. Zeta-Potential measurements of POPG/TOCL (filled squares) and DMPG/TMCL (empty squares) each in a molar ratio of 80:20 in absence and presence of SAAP-148 (A), OP-145 (B) and I12K (C) at indicated concentrations ranging from 0.5 to 8 µM. Data are summary of three independent experiments.

As expected, the Zeta-potential of the pure membrane models POPG/TOCL and DMPG/TMCL does not differ and shows a value of -30 mV. Addition of the peptides changes the Zeta-potential of both model membranes towards neutralization and leads to an overcompensation at higher peptide concentrations, especially for OP-145 and SAAP-148. There is no difference between POPG/TOCL and DMPG/TMCL measurements in the presence of the peptides. In agreement with data observed for POPG lipid vesicles, SAAP-148 is the peptide with the highest neutralization potential (2.5 µM for POPG/TOCL, 5 µM for DMPG/TMCL). For OP-145, a higher peptide concentration is needed to neutralize surface charge in comparison to SAAP-148, which is about 6 µM for both model membrane systems. I12K neutralizes the surface charge at 8 µM concerning POPG/TOCL and 16 µM for DMPG/TMCL.

3.3.2. MEMBRANE PERMEABILITY

To examine bilayer permeability of the model system, fluorescence-based leakage experiments were performed. Large unilamellar vesicles composed of POPG as well as POPG and TOCL in a molar ratio of 80 to 20 were used loaded with ANTS/DPX and incubated with each peptide (OP-145, SAAP-148, I12K). The peptides were added in incremental amounts ranging from 0.25 to 8 µM. Triton (1%) acts as positive control and indicates 100% leakage.

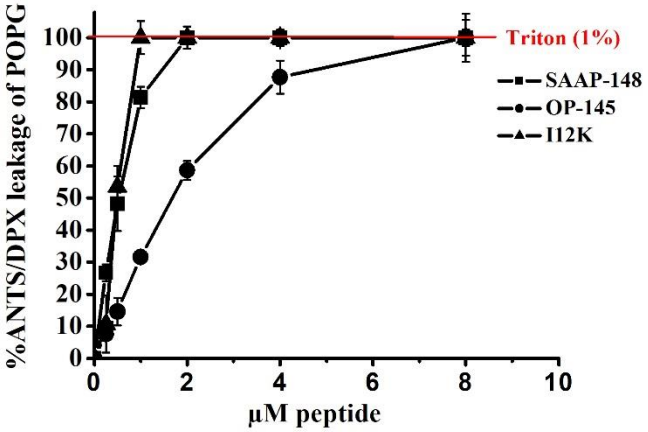

Figure 14. Effect of SAAP-148, OP-145 and I12K on bacterial membrane mimics. Leakage of LUVs composed of POPG at indicated peptide concentrations (SAAP-148 (squares), OP-145 (circles), I12K (triangles)) in the range of 0.25 to 8 µM. Red line represents full leakage. Data are the summary of three independent experiments.

Release of enclosed fluorescence marker molecules from POPG is observed already at the lowest concentration for all peptides tested (0.25 µM). I12K reaches full leakage at 1 µM. For SAAP-148-treated liposomes, full leakage is reached at 2 µM. 8 µM of OP-145 induce 100% membrane leakage of POPG vesicles. By comparing these data with leakage data from the lipid

mixture POPG/TOCL, it is evident that for POPG/TOCL lipid vesicles the peptide demand for membrane permeabilization is not that high as for POPG liposomes.

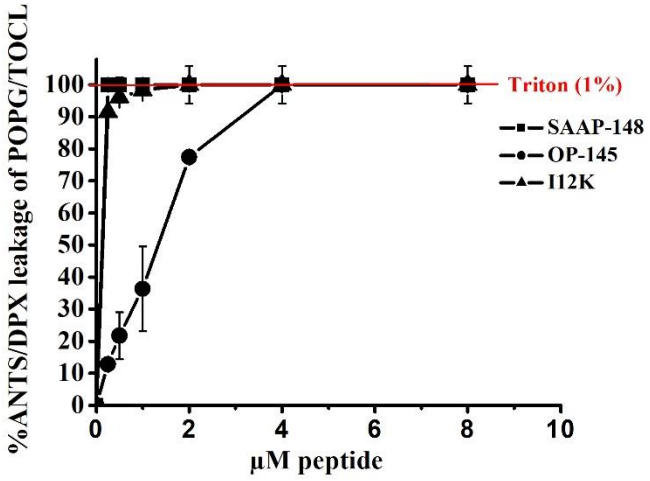

Figure 15. Effect of SAAP-148, OP-145 and I12K on bacterial membrane mimics. Leakage of LUVs composed of POPG/TOCL at indicated peptide concentrations (SAAP-148, OP-145, I12K) in the range of 0.25 to 8 µM. Red line represents full leakage. Data are the summary of three independent experiments.

Release of enclosed fluorescence marker molecules from POPG/TOCL is observed already at the lowest concentration tested (0.25 µM). For SAAP-148-treated liposomes, full leakage is achieved at 0.5 µM. At this concentration, I12K almost permeabilizes the bilayer. It reaches full leakage at 2 µM. At a total concentration of 4 µM OP-145, 100% membrane leakage from POPG/TOCL vesicles is obtained.

Stronger permeabilization is achieved for CL containing membranes by all three peptides. This effect might be ascribed to the stronger interaction of the cationic peptides with CL as already mentioned by Malanovic and Lohner [3]. Furthermore, I12K is most efficient on POPG liposomes and permeabilizes the membrane at 1 µM (SAAP-148: 2 µM), whereby for POPG/TOCL liposomes SAAP-148 causes 100% leakage before I12K at 0.5 µM (I12K: 2 µM). OP-145 exhibits least permeabilization efficiency, although it needs 8 µM of OP-145 for full leakage of POPG liposomes, which is twice as much peptide as for POPG/TOCL liposomes.

3.3.3. THERMODYNAMIC STUDIES WITH THE MODEL MEMBRANE DMPG/TMCL

To assess how the peptides OP-145, SAAP-148 and I12K interact with the lipid membrane, differential scanning calorimetry was performed using the membrane mimic DMPG/TMCL (80:20) as well as pure DMPG and TMCL. Measurements were done before and after exposure to the peptides, in the molar lipid-to-peptide ratios of 100:1 and 25:1. For each sample, six

scans were done, three heating and three cooling scans from 1 to 75°C with a scan rate of 0.5°C/min. Figure 16 shows the fifth scan of each measurement, which is representative for all six scans of one measurement. The exact transition temperatures and their corresponding enthalpies are presented in Table 3. Due to overlapping domains in some measurements, only the total enthalpy could be accurately calculated.

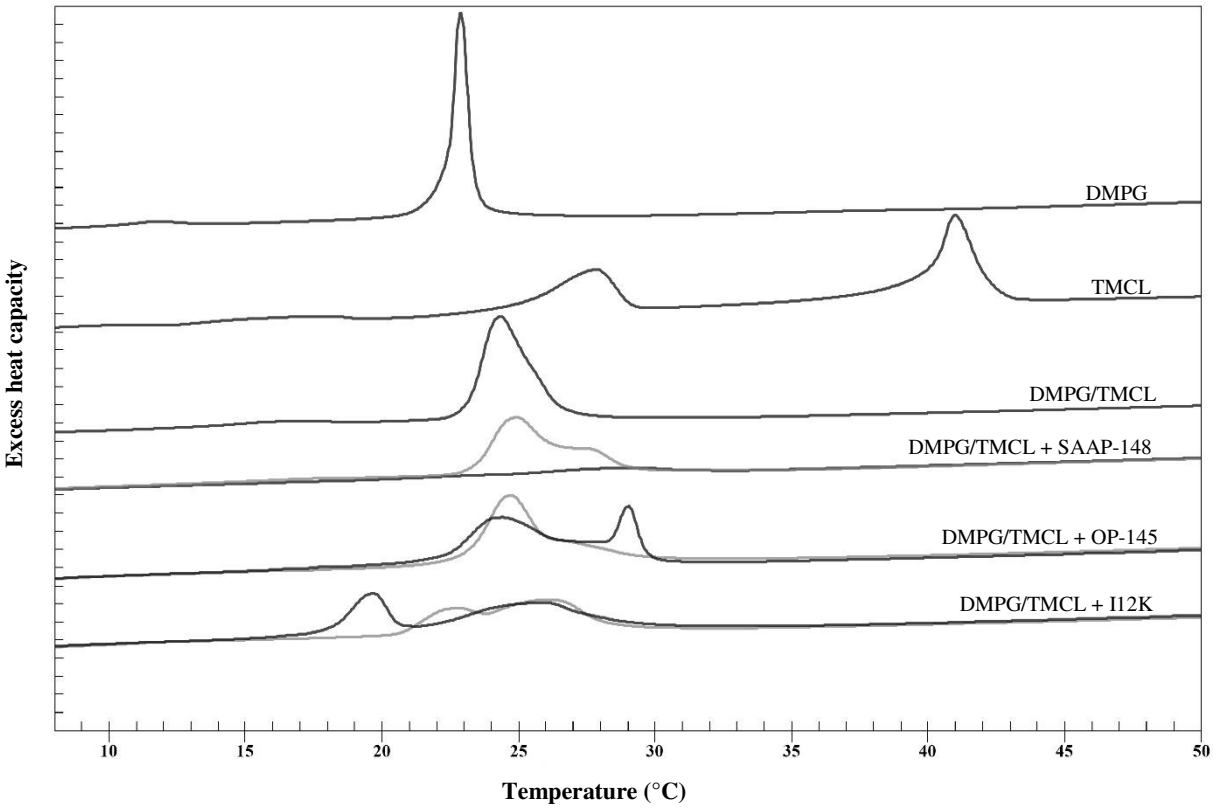

Figure 16. Thermotropic behavior of DMPG, TMCL and DMPG/TMCL (80:20) vesicles and peptide dependent thermotropic behavior of DMPG/TMCL (80:20) vesicles in the presence of SAAP-145, OP-145 and I12K as observed in heating scans. Grey lines indicate the molar lipid-to-peptide ratio of 100:1, black lines stand for 25:1.

Table 3. Thermodynamic parameters (low-temperature transition, pretransition and main transition temperature ($T_{low}/T_{pre}/T_m$) and corresponding enthalpies ($\Delta H_{low}/\Delta H_{pre}/\Delta H_m$)) of DMPG, TMCL and DMPG/TMCL (80:20) liposomes in the presence and absence of the peptides SAAP-148, OP-145 and I12K in the molar ratios 25:1 and 100:1 (lipid:peptide).

	T_{low} (°C)	ΔH_{low} (kcal/mol)	T_{pre} (°C)	ΔH_{pre} (kcal/mol)	T_m (°C)	ΔH_m (kcal/mol)
DMPG			12.0	1.0	22.9	7.9
TMCL	17.9	4.7	27.9	3.8	41.0	17.3

DMPG/TMCL		24.4	9.9
DMPG/TMCL + SAAP-148			
100:1		24.8	10.1
25:1		28.3	2.1
DMPG/TMCL + OP-145			
100:1		25.0	8.0
25:1		24.3; 29.1	16.1 *
DMPG/TMCL + I12K			
100:1		22.7; 26.1	9.70 *
25:1		19.7; 25.9	14.7 *

* total enthalpy

In accordance with reported data [41], three well-separated phase transitions can be observed for TMCL. The low temperature transition (T_{low}) from the subsubgel phase (metastable gel phase with tilted fatty acids) to the lamellar gel phase is at 17.9°C. The pre-transition temperature (T_{pre}) from the lamellar gel to the ripple phase is at 27.9°C. The main transition (T_m) to the fluid phase occurs at 41.0°C. DMPG shows two transitions, the pre-transition at 12.0°C and the main transition at 22.9°C. As a consequence of the lipid composition of DMPG/TMCL and its molar ratio of 80 to 20, the temperature of the phase transition is located nearby the temperature of pure DMPG at 24.4°C. No pre- and low temperature transitions were detected for DMPG/TMCL. Every peptide has a different effect on the membrane model DMPG/TMCL. However, each peptide within the lipid-to-peptide ratio of 100:1 does not induce a remarkable shift of the main transition temperature. SAAP-148 (L:P = 100:1) leads to an induction of domain formation with the total enthalpy of 10.1, which is quite consistent to untreated membranes (ΔH_m = 9.9), whereby the transition temperature slightly increases to 24.8°C. However, for SAAP-148 at a ratio of 25:1 hardly a transition could be detected. A very

small transition at higher temperatures at 28.3°C with an enthalpy of 2.1 kcal/mol can be observed, which may result from the formation of small vesicular structures rich in CL [3] or micellar structures [33]. For both, OP-145 and I12K (L:P = 25:1) an indication for phase separation resulting from the appearance of a very broad transition is also detected at 100:1 molar ratio (OP-145: T_m = 25.0°C; I12K: T_m = 26.1°C) and stronger pronounced at 25:1. Interestingly, the phase separation induced by OP-145 is shifting to higher temperatures of 29.1°C, in the direction of that from pure TMCL, whereas with I12K the shift to 19.7°C tends towards pure DMPG. These findings indicate that I12K preferentially interacts with CL. Both peptides at the ratio of 25:1 induce an increase of the enthalpy and the main transition temperature, which indicates a stabilization of the gel phase due to tighter lipid packing.

4. DISCUSSION

Bacterial killing induced by AMPs is a good strategy to combat the enormous increase of multidrug resistant bacterial strains. Because of their cationic properties, AMPs are thought to be targeting anionic phospholipids on the bacterial membrane surface. Malanovic et al. reported that this may lead to membrane perturbation, eventually rupture and cell death [2]. According to de Breij et al. [4], many antimicrobial peptides supposedly target the bacterial cytoplasmic membrane leading to membrane disruption and disorder, consequently leading to death [4]. The major lipid species of *Enterococcus hirae* contain negatively charged PG and CL and a small number of neutral lipids (Malanovic et al. unpublished). This study should be the foundation for further studies concerning pathogenic Gram-positive bacteria. In this context, the main finding of the present study is the mechanism of the three AMPs OP-145, SAAP-148 and I12K upon interaction with bacteria. Here, we report that all three peptides are effective against *E. hirae* to a different extent.

In accordance with an earlier report on *S. aureus* [2] OP-145 showed killing effects against *E. hirae* at 3.2 µM within 5 minutes, whereas the $LC_{99.9\%}$ of *S. aureus* is at 1.6 µM. At killing concentrations, only 27% membrane permeabilization and 50% membrane depolarization could be detected regarding *E. hirae* live cells. SAAP-148 exhibited more potent antimicrobial activity against *E. hirae* at 0.1 µM. According to de Breij et al. [4], SAAP-148 is a highly effective antimicrobial peptide against Gram-negative ESKAPE and MDR Gram-positive pathogens by permeabilizing the bacterial cytoplasmic membrane [4]. One big difference between OP-145 and SAAP-148 is the required peptide concentration. SAAP-148 kills bacteria at a significantly lower concentration than OP-145. This can be ascribed to the higher positive net charge of SAAP-148 of +11, while OP-145 has a net charge of +6. Thus, using SAAP-148 electrostatic interactions are stronger between the cationic peptide and the anionic lipid head groups, which leads to faster neutralization and consequently a faster cell death [2,4]. The $LC_{99.9\%}$ of 0.1 µM caused a membrane depolarization of *E. hirae* of about 55%, whereby this low concentration was not evaluated regarding membrane permeabilization. However, at 0.4 µM SAAP-148 permeabilized 83% of the bacterial membrane. In contrast to OP-145 and SAAP-148, I12K kills bacteria at a much higher concentration of about 102.4 µM after 20 minutes of incubation. This could possibly be a consequence of the breaking the hydrophobic face as well as the helical structure of the peptide shown in Figure 3 which prevents the peptide's insertion into the cell

membrane. I12K has rather the ability to interact with other components or it remains outside the plasma membrane. Apparently, I12K has only little effect on the membrane permeabilization of *E. hirae* as it is leading to only 5% at 102.4 µM after 20 minutes. 51.2 µM of I12K caused 30% membrane depolarization. In sum, killing of bacteria occurs before total membrane disruption. Comparing these findings with results from the Gram-negative bacterial strain *E. coli* (master thesis Ayse Ön), the following observations are noticeable: OP-145 and SAAP-148 kill *E. hirae* at a significantly lower concentration than *E. coli* while the $LC_{99.9\%}$ of I12K is much higher for *E. hirae* than it is for *E. coli*. Membrane permeabilization data of OP-145 coincides for both bacterial strains. SAAP-148 and I12K do not exhibit that high permeabilization potential against *E. hirae* as they do for *E. coli*. These differences might be explained by the different membrane composition of diverse bacterial strains [11]. However, SAAP-148 permeabilizes the plasma membrane of *S. aureus* rapidly. As reported by de Breij et al., ≥ 0.8 µM of SAAP-148 lead to more than 90% membrane permeabilization within 60 seconds [4].

For peptide treated *E. hirae* cells, no neutralization of the surface charge could be detected. According to earlier studies with the Gram-negative bacterial strain *E. coli* (data not shown), the opposite occurs as the surface charge is neutralized before the cells are killed. The thick LPS layer of Gram-negative bacteria might be a reason explaining surface neutralization due to the interaction of negatively charged LPS with the peptides. Because Gram-positive bacteria lack this LPS layer [11], the peptide might penetrate toward the membrane without foregoing neutralization or interaction with the cell wall components. Further, the high hydrophobicity of the peptides, in particular SAAP-148 facilitates strong partitioning and insertion into the membrane. However, no full membrane depolarization and permeabilization were reached. Moreover, I12K also did not affect the surface charge of *E. hirae*, which consequently eliminates the possibility of interaction with the negatively charged surface component LTA and rather suggests that the peptide remains somewhere in the peptidoglycan mesh.

The microscopy findings of the *E. hirae* wildtype displayed a homogenous Nile Red incorporation across the cell membrane with intensively staining at the septal region, which might indicate the elevated concentration of CL and PG as already shown by Agrawal et al. for exponentially growing *E. coli* cells [40]. Lipid domains enriched in CL are located at the septum and the pole as described for *Bacillus subtilis*, *Pseudomonas putida* and *Enterococcus faecalis*

[3,42]. Peptide treated cells exhibited at either one or both septal poles a big Nile Red dot, whereby in some cases the dots appeared elsewhere in the membrane. It is suggested that the anionic lipid PG may guide the initial attack in the polar and septal regions by the cationic AMP [40]. PG might lead the polar permeabilization of the cytoplasmic membrane, but not CL, since PG is able to distribute its anionic charges more flexible and in turn, accommodates better than the bulky tails of CL [40,43]. Indeed, it was shown by Pogmore et al. that *Bacillus subtilis* does not form CL specific domains [43]. For instance, LL-37 locally initiates outer and cytoplasmic membrane permeabilization at the septum or at one endcap [40]. As all three peptides OP-145, SAAP-148 and I12K are derived from LL-37, they may display the same behavior as observed in Figure 11, whereby for I12K a homogenous dot distribution over the membrane and a consistent incorporation across the septal regions is remarkable. At increased concentrations of OP-145 and SAAP-148, changes in membrane fluidity were strongly enhanced. We also cannot exclude that the effect of the disturbed membrane fluidity and the subsequent cell death may be accompanied or enhanced by autolysin activation in the membrane caused by the interaction of the AMPs with the membrane. Besides these findings, a diminished cell volume of the bacterial cells can be observed for all three peptides, which further supports the formation of pores by the loss of intracellular content. The shrinkage of the cells might be ascribed to the loss of the cell's turgor pressure.

The assumption about the pore-forming mechanism is supported by the leakage and Zeta-potential data of the membrane models POPG/TOCL and POPG mimicking the inner plasma membrane of *E. hirae* since no coverage of the membrane surface by the peptides is necessary for induction of the transmembrane pore formation and can emerge below the threshold concentration [33]. Within this study, it has not been clarified if the peptides are oriented perpendicularly to the bilayer as proposed for pore forming mechanisms by Kumar et al. [9] and Lohner [33]. 100% leakage of POPG/TOCL is reached at 0.5 µM SAAP-148, 2 µM I12K and 4 µM OP-145, whereas higher peptide concentrations are necessary for full leakage of POPG (2 µM SAAP-148, 1 µM I12K and 8 µM OP-145). These data propose that besides electrostatic interactions also hydrophobic interactions play a key role between the model membranes and OP-145 and SAAP-148, leading to full membrane permeabilization at low peptide concentrations[3]. Whereby OP-145 requires higher peptide concentrations for full membrane leakage than SAAP-148. Moreover, the lysin of I12K may lead to an additional membrane perturbation of the hydrophobic site.

For all three membrane models POPG, POPG/TOCL and DMPG/TMCL the same trend from a negative Zeta-potential (- 40 mV) towards a neutral/positive surface charge is detectable. Concerning OP-145 and I12K, higher peptide concentrations are required for surface charge neutralization than for SAAP-148. At these concentrations, the membrane is already fully permeabilized. Only when reaching higher peptide concentrations above 2 µM for SAAP-148, 6 µM for OP-145 and 6-8 µM for I12K the peptides stay outside the membrane causing a differently pronounced charge overcompensation. At the end concentration of 8 µM SAAP-148 reaches about 20 mV, OP-145 about 15 mV and I12K altered the Zeta-potential to a value just slightly above zero. Here again, present results suggest that the peptides' mode of action might be the formation of pores. This assumption is supported by the rapid initial membrane permeabilization followed by an overcompensation outside the membrane only at higher peptide concentrations where full leakage is already reached.

As described by Lohner differential scanning calorimetry is a widely used method for phase transition studies and conformational alterations in biological systems as nucleic acids, proteins and lipid assemblies [44]. At a lipid:peptide molar ratio of 25:1 SAAP-148 caused a loss of the cooperative gel-fluid phase transition of PG/CL resulting in a broad uncooperative phase transition with very low enthalpy, which may be indicative for small lipid-peptide aggregates as already shown for δ-lysin [44,45], LL-37 [45] and OP-145 [2]. Micellization of liposomes at increasing peptide concentrations [32] has already been reported for liposomes composed of PC [33]. OP-145 and I12K induce lipid phase segregation by interacting preferably with one of the two anionic lipids. OP-145 causes a shift towards higher temperatures, I12K towards lower temperatures. Generally, phospholipids are packed tighter in the gel phase, where the peptide's ability to interact with the lipids decreases [44], which might be reflected in the decreased antimicrobial activity of I12K compared to OP-145 and SAAP-148.

In summary, the present results demonstrate that OP-145 and SAAP-148 are targeting the cell membrane of *E. hirae*. They are effective antimicrobial peptides by killing *Enterococcus hirae*, whereby SAAP-148 is a stronger AMP as it neutralizes the membrane surface faster and kills bacteria at a significantly lower concentration than OP-145. I12K exhibits very weak bactericidal activity against *E. hirae*. It is proposed that the first stage of action can be characterized by adsorption of the peptides without preceding surface charge neutralization of the outer cell wall components or any coverage by the peptides. In the second stage, the peptides interact

with the plasma membrane causing a loss of cytoplasmic material at defined areas of the membrane leading to shrinkage of the cells. We suggest that the disruption of the bacterial membrane by OP-145, SAAP-148 and I12K will most likely occur by pore formation as it does for melittin, magainin2 or aurein 2.2 [9]. Whether this pore-forming mechanism leads to membrane thinning or thickening as described for PGLa [33] was not part of the biophysical experiments performed in this study. Moreover, discrimination between barrel stave and toroidal pore model [32] cannot be carried out yet. Furthermore, the differences in membrane fluidity are an indication for a different distribution of lipids and in turn of the peptides at specific sites in the membrane supported by the lipid segregation observed in model membranes. Further biophysical parameters should be considered to understand the effect of the tested AMPs better and approve the study's findings. Possibilities for further investigations would be ITC analysis providing information about the binding affinity, a quantitative determination of the lipid bilayer or a comprehensive bilayer structure analysis via X-Ray.

ABBREVIATIONS

AMP	antimicrobial peptide
ANTS	8-aminonaphthalene-1.3.6-trisulfonic acid
ATCC	american type culture collection
BAI	biomaterial-associated infections
BHIB	Brain-Heart-Infusion Broth
CD	circular dichroism
CFU	colony forming unit
CL	cardiolipin
CWA	cell wall anchored
DMPG	1,2-dimyristoyl-sn-glycero-3-phospho-(1'-rac-glycerol) (sodium salt) (14:0 PG)
DPX	p-xylene-bis-pyridinium bromide
DSC	differential scanning calorimetry
E. coli	*Escherichia coli*
E. faecalis	*Enterococcus faecalis*
E. faecium	*Enterococcus faecium*
E. hirae	*Enterococcus hirae*
ESKAPE	*Enterococcus faecium*, *Staphylococcus aureus*, *Klebsiella pneumoniae*, *Acinetobacter baumannii*, *Pseudomonas aeruginosa* and *Enterobacter* species
HEPES	4-(2-Hydroxyethyl) piperazine-1-ethanesulfonic acid
ITC	isothermal titration calorimetry
LC	lethal concentration (≥ 99.9%)
LPS	lipopolysaccharides
LTA	lipoteichoic acid
LUV	large unilamellar vesicle
MDR	multidrug-resistant
MRSA	methicillin resistant *Staphylococcus aureus*
MurNAc-GlcNAc	*N*-acetylmuramic acid-(β1-4)-*N*-acetylglucosamine
NaPi	sodium phosphate buffer

OD	optical density
PC	phosphatidylcholine
PG	phosphatidylglycerol
PGN	peptidoglycan
PI	propidium iodide
POPG	1-palmitoyl-2-oleoyl-sn-glycero-3-phospho-(1'-rac-glycerol)
S. aureus	*Staphylococcus aureus*
T_{low}	low-temperature transition
T_m	main transition temperature
TMCL	1',3'-bis[1,2-dimyristoyl-sn-glycero-3-phospho]-glycerol
TOCL	1',3'-bis[1,2-dioleoyl-sn-glycero-3-phospho]-glycerol
T_{pre}	pretransition temperature
WT	wildtype
WTA	cell wall teichoic acid
ΔH	enthaply

REFERENCES

References

[1]K. Lohner, New strategies for novel antibiotics: peptides targeting bacterial cell membranes, gpb 28 (2009) 105–116.

[2]N. Malanovic, R. Leber, M. Schmuck, M. Kriechbaum, R.A. Cordfunke, J.W. Drijfhout, A. de Breij, P.H. Nibbering, D. Kolb, K. Lohner, Phospholipid-driven differences determine the action of the synthetic antimicrobial peptide OP-145 on Gram-positive bacterial and mammalian membrane model systems, Biochimica et biophysica acta 1848 (2015) 2437–2447.

[3]N. Malanovic, K. Lohner, Antimicrobial Peptides Targeting Gram-Positive Bacteria, Pharmaceuticals (Basel, Switzerland) 9 (2016).

[4]A. de Breij, M. Riool, R.A. Cordfunke, N. Malanovic, L. de Boer, R.I. Koning, E. Ravensbergen, M. Franken, T. van der Heijde, B.K. Boekema, P.H.S. Kwakman, N. Kamp, A. El Ghalbzouri, K. Lohner, S.A.J. Zaat, J.W. Drijfhout, P.H. Nibbering, The antimicrobial peptide SAAP-148 combats drug-resistant bacteria and biofilms, Science translational medicine 10 (2018).

[5]W.H. Organization, Antimicrobial Resistance: Global Report on Surveillance, World Health Organization, Geneva, 2014.

[6]A.R. von Gundlach, V.M. Garamus, T. Gorniak, H.A. Davies, M. Reischl, R. Mikut, K. Hilpert, A. Rosenhahn, Small angle X-ray scattering as a high-throughput method to classify antimicrobial modes of action, Biochimica et biophysica acta 1858 (2016) 918–925.

[7]G. Kapoor, S. Saigal, A. Elongavan, Action and resistance mechanisms of antibiotics: A guide for clinicians, Journal of anaesthesiology, clinical pharmacology 33 (2017) 300–305.

[8]G. Wang, X. Li, Z. Wang, APD3: the antimicrobial peptide database as a tool for research and education, Nucleic acids research 44 (2016) D1087-93.

[9]P. Kumar, J.N. Kizhakkedathu, S.K. Straus, Antimicrobial Peptides: Diversity, Mechanism of Action and Strategies to Improve the Activity and Biocompatibility In Vivo, Biomolecules 8 (2018).

[10]R.M. Epand, H.J. Vogel, Diversity of antimicrobial peptides and their mechanisms of action, Biochimica et biophysica acta 1462 (1999) 11–28.

[11]N. Malanovic, K. Lohner, Gram-positive bacterial cell envelopes: The impact on the activity of antimicrobial peptides, Biochimica et biophysica acta 1858 (2016) 936–946.

[12]A. de Breij, M. Riool, P.H.S. Kwakman, L. de Boer, R.A. Cordfunke, J.W. Drijfhout, O. Cohen, N. Emanuel, S.A.J. Zaat, P.H. Nibbering, T.F. Moriarty, Prevention of Staphylococcus aureus biomaterial-associated infections using a polymer-lipid coating containing the antimicrobial

peptide OP-145, Journal of controlled release : official journal of the Controlled Release Society 222 (2016) 1–8.

[13]H.G. Boman, Antibacterial peptides: basic facts and emerging concepts, Journal of internal medicine 254 (2003) 197–215.

[14]L. Ming, J.-A. Huang, The Antibacterial Effects of Antimicrobial Peptides OP-145 against Clinically Isolated Multi-Resistant Strains, Japanese journal of infectious diseases 70 (2017) 601–603.

[15]U.H.N. Dürr, U.S. Sudheendra, A. Ramamoorthy, LL-37, the only human member of the cathelicidin family of antimicrobial peptides, Biochimica et biophysica acta 1758 (2006) 1408–1425.

[16]J.M. Kahlenberg, M.J. Kaplan, Little peptide, big effects: the role of LL-37 in inflammation and autoimmune disease, Journal of immunology (Baltimore, Md. : 1950) 191 (2013) 4895–4901.

[17]F. Porcelli, R. Verardi, L. Shi, K.A. Henzler-Wildman, A. Ramamoorthy, G. Veglia, NMR structure of the cathelicidin-derived human antimicrobial peptide LL-37 in dodecylphosphocholine micelles, Biochemistry 47 (2008) 5565–5572.

[18]M.F. Burton, P.G. Steel, The chemistry and biology of LL-37, Natural product reports 26 (2009) 1572–1584.

[19]D.J. Schibli, R.F. Epand, H.J. Vogel, R.M. Epand, Tryptophan-rich antimicrobial peptides: comparative properties and membrane interactions, Biochemistry and cell biology = Biochimie et biologie cellulaire 80 (2002) 667–677.

[20]M.J. Nell, G.S. Tjabringa, A.R. Wafelman, R. Verrijk, P.S. Hiemstra, J.W. Drijfhout, J.J. Grote, Development of novel LL-37 derived antimicrobial peptides with LPS and LTA neutralizing and antimicrobial activities for therapeutic application, Peptides 27 (2006) 649–660.

[21]E.M. Haisma, A. de Breij, H. Chan, J.T. van Dissel, J.W. Drijfhout, P.S. Hiemstra, A. El Ghalbzouri, P.H. Nibbering, LL-37-derived peptides eradicate multidrug-resistant Staphylococcus aureus from thermally wounded human skin equivalents, Antimicrobial agents and chemotherapy 58 (2014) 4411–4419.

[22]B. Bechinger, S.-U. Gorr, Antimicrobial Peptides: Mechanisms of Action and Resistance, Journal of dental research 96 (2017) 254–260.

[23]M.N. Melo, R. Ferre, M.A.R.B. Castanho, Antimicrobial peptides: linking partition, activity and high membrane-bound concentrations, Nature reviews. Microbiology 7 (2009) 245–250.

[24]P.V. Dicpinigaitis, M. de Aguirre, J. Divito, Enterococcus hirae Bacteremia Associated with Acute Pancreatitis and Septic Shock, Case reports in infectious diseases 2015 (2015) 123852.

[25]R. Anghinah, R.G.S. Watanabe, M.M. Simabukuro, C. Guariglia, L.F. Pinto, D.C.d.M.E. Gonçalves, Native Valve Endocarditis due to Enterococcus hirae Presenting as a Neurological Deficit, Case reports in neurological medicine 2013 (2013) 636070.

[26]A.L. Koch, Bacterial Growth and Form, Springer Netherlands, 2013.

[27]L.E. Hancock, B.E. Murray, J. Sillanpää, Enterococci: From Commensals to Leading Causes of Drug Resistant Infection: Enterococcal Cell Wall Components and Structures, Boston, 2014.

[28]R.E. Lehotzky, C.L. Partch, S. Mukherjee, H.L. Cash, W.E. Goldman, K.H. Gardner, L.V. Hooper, Molecular basis for peptidoglycan recognition by a bactericidal lectin, Proceedings of the National Academy of Sciences of the United States of America 107 (2010) 7722–7727.

[29]G.D. Shockman, J.T. Martin, Autolytic enzyme system of Streptococcus faecalis. IV. Electron microscopic observations of autolysin and lysozyme action, Journal of bacteriology 96 (1968) 1803–1810.

[30]G.D. Shockman, The autolytic ('suicidase') system of Enterococcus hirae: From lysine depletion autolysis to biochemical and molecular studies of the two muramidases of Enterococcus hirae ATCC 9790, FEMS Microbiology Letters (1992).

[31]J.M. Monteiro, P.B. Fernandes, F. Vaz, A.R. Pereira, A.C. Tavares, M.T. Ferreira, P.M. Pereira, H. Veiga, E. Kuru, M.S. VanNieuwenhze, Y.V. Brun, S.R. Filipe, M.G. Pinho, Cell shape dynamics during the staphylococcal cell cycle, Nature communications 6 (2015) 8055.

[32]B. Bechinger, K. Lohner, Detergent-like actions of linear amphipathic cationic antimicrobial peptides, Biochimica et biophysica acta 1758 (2006) 1529–1539.

[33]K. Lohner, Novel Antibiotics Based upon the Multiple Mechanisms of Membrane Perturbation by Antimicrobial Peptides, Current Topics in Medicinal Chemistry (2016).

[34]C.-F. Le, C.-M. Fang, S.D. Sekaran, Intracellular Targeting Mechanisms by Antimicrobial Peptides, Antimicrobial agents and chemotherapy 61 (2017).

[35]D. Koller, K. Lohner, The role of spontaneous lipid curvature in the interaction of interfacially active peptides with membranes, Biochimica et biophysica acta 1838 (2014) 2250–2259.

[36]K. Scheinpflug, M. Wenzel, O. Krylova, J.E. Bandow, M. Dathe, H. Strahl, Antimicrobial peptide cWFW kills by combining lipid phase separation with autolysis, Scientific reports 7 (2017) 44332.

[37]D. Zweytick, G. Deutsch, J. Andrä, S.E. Blondelle, E. Vollmer, R. Jerala, K. Lohner, Studies on lactoferricin-derived Escherichia coli membrane-active peptides reveal differences in the mechanism of N-acylated versus nonacylated peptides, The Journal of biological chemistry 286 (2011) 21266–21276.

[38]M.M. Domingues, M.A.R.B. Castanho, N.C. Santos, rBPI(21) promotes lipopolysaccharide aggregation and exerts its antimicrobial effects by (hemi)fusion of PG-containing membranes, PloS one 4 (2009) e8385.

[39]J.M. Freire, M.M. Domingues, J. Matos, M.N. Melo, A.S. Veiga, N.C. Santos, M.A.R.B. Castanho, Using zeta-potential measurements to quantify peptide partition to lipid membranes, European biophysics journal : EBJ 40 (2011) 481–487.

[40]A. Agrawal, N. Rangarajan, J.C. Weisshaar, Resistance of early stationary phase E. coli to membrane permeabilization by the antimicrobial peptide Cecropin A, Biochimica et biophysica acta. Biomembranes (2019).

[41]F. Prossnigg, A. Hickel, G. Pabst, K. Lohner, Packing behaviour of two predominant anionic phospholipids of bacterial cytoplasmic membranes, Biophysical chemistry 150 (2010) 129–135.

[42]H. Strahl, J. Errington, Bacterial Membranes: Structure, Domains, and Function, Annual review of microbiology 71 (2017) 519–538.

[43]A.-R. Pogmore, K.H. Seistrup, H. Strahl, The Gram-positive model organism Bacillus subtilis does not form microscopically detectable cardiolipin-specific lipid domains, Microbiology (Reading, England) 164 (2018) 475–482.

[44]K. Lohner, E. Staudegger, E.J. Prenner, R.N. Lewis, M. Kriechbaum, G. Degovics, R.N. McElhaney, Effect of staphylococcal delta-lysin on the thermotropic phase behavior and vesicle morphology of dimyristoylphosphatidylcholine lipid bilayer model membranes. Differential scanning calorimetric, 31P nuclear magnetic resonance and Fourier transform infrared spectroscopic, and X-ray diffraction studies, Biochemistry 38 (1999) 16514–16528.

[45]E. Sevcsik, G. Pabst, A. Jilek, K. Lohner, How lipids influence the mode of action of membrane-active peptides, Biochimica et biophysica acta 1768 (2007) 2586–2595.